The Company of **Biologists**

Development of a 3D atlas of the embryonic pancreas for topological and quantitative analysis of heterologous cell interactions

Laura Glorieux[1,*], Aleksandra Sapala[2,3,*], David Willnow[4,*], Manon Moulis[1], Anna Salowka[4], Jean-Francois Darrigrand[4], Shlomit Edri[5], Anat Schonblum[6], Lina Sakhneny[6], Laura Schaumann[2,3], Harold F. Gómez[2,3], Christine Lang[2,3], Lisa Conrad[2,3], Fabien Guillemot[7], Shulamit Levenberg[5], Limor Landsman[6], Dagmar Iber[2,3,‡,§], Christophe E. Pierreux[1,‡,§] and Francesca M. Spagnoli[4,‡,§]

ABSTRACT

Generating comprehensive image maps, while preserving spatial three-dimensional (3D) context, is essential in order to locate and assess quantitatively specific cellular features and cell-cell interactions during organ development. Despite recent advances in 3D imaging approaches, our current knowledge of the spatial organization of distinct cell types in the embryonic pancreatic tissue is still largely based on two-dimensional histological sections. Here, we present a light-sheet fluorescence microscopy approach to image the pancreas in three dimensions and map tissue interactions at key time points in the mouse embryo. We demonstrate the utility of the approach by providing volumetric data, 3D distribution of three main cellular components (epithelial, mesenchymal and endothelial cells) within the developing pancreas, and quantification of their relative cellular abundance within the tissue. Interestingly, our 3D images show that endocrine cells are constantly and increasingly in contact with endothelial cells forming small vessels, whereas the interactions with mesenchymal cells decrease over time. These findings suggest distinct cell-cell interaction requirements for early endocrine cell specification and late differentiation. Lastly, we combine our image data in an open-source online repository (referred to as the Pancreas Embryonic Cell Atlas).

INTRODUCTION

Organogenesis is a finely tuned process, involving the expansion and differentiation of organ-specific progenitor cell populations in the context of profound morphological changes in the tissue architecture (Zorn and Wells, 2009). The formation of an organ relies on the precise activation of cell-intrinsic differentiation programs, but also on the interaction of progenitor cell populations with surrounding tissues. These cell-cell interactions provide essential cues to guide cell differentiation and tissue morphogenesis in a spatially and temporally defined fashion. Full comprehension of these events will help to elucidate the mechanisms underpinning tissue formation, but also guide bioengineering strategies to build three-dimensional (3D) tissue models (Bulanova et al., 2017; Iber et al., 2016; Kaufman-Francis et al., 2012).

The pancreas represents a paradigmatic example of how tissue-intrinsic cell-cell interactions and extrinsic signals released from surrounding non-pancreatic tissues, such as mesenchyme and blood vessels, coordinate cell differentiation and morphogenesis to form a fully functional adult organ (Cozzitorto and Spagnoli, 2019; Larsen and Grapin-Botton, 2017; Pan and Wright, 2011; Shih et al., 2013; Wessells and Cohen, 1967). The adult pancreas is an amphicrine gland; the exocrine compartment produces and releases the digestive enzymes, whereas the endocrine compartment houses the insulin-secreting β-cells and is crucial for blood glucose homeostasis (Sneddon et al., 2018). Remarkably, all pancreatic cell types, including the acinar, ductal and endocrine cells, derive from a common pool of endoderm progenitors, which is specified in the mouse around embryonic day (E) 8.5 (Gittes, 2009; Zorn and Wells, 2009). Recent studies have shown that pancreatic epithelium morphogenesis begins with the remodeling of a globular mass of non-polarized epithelial cells at E11.5 (Pan and Wright, 2011). Acquisition of apical-basal epithelial polarity together with the coalescence of multiple microlumens represent the initial steps underlying the formation of a branched monolayered epithelium that subsequently differentiates into ducts and acini (Hick et al., 2009; Kesavan et al., 2009; Villasenor et al., 2010). Afterwards, further branching and expansion of the pancreatic ducts occur by iterative lateral branching. Tubulogenesis and branching in the developing pancreas, as in other epithelial organs, coincide with growth and fate specification. Between E12.5 and E14.5, the pancreatic epithelium undergoes important remodeling events, which result in the formation of a tubular network called the plexus, with a proximo-distal 'tip and trunk' domain organization (Bankaitis et al., 2015; Larsen et al., 2017; Pan and Wright, 2011; Pierreux et al., 2010; Sznurkowska et al., 2018; Villasenor et al., 2010; Zhou et al., 2007). Regions at the periphery of the pancreatic epithelium consist of elongating branch tips, whereas the center contains the luminal plexus and corresponds to trunk domains. Importantly, such proximo-distal architecture coincides with cell fate restriction of pancreatic progenitors and

[1]Cell Biology Unit, de Duve Institute, UCLouvain, Woluwe 1200, Belgium. [2]Department of Biosystems Science and Engineering (D-BSSE), ETH Zurich, Basel 4058, Switzerland. [3]Swiss Institute of Bioinformatics (SIB), Basel 4058, Switzerland. [4]Centre for Stem Cell and Regenerative Medicine, King's College London, Great Maze Pond, London SE1 9RT, UK. [5]Department of Biomedical Engineering, Technion–Israel Institute of Technology, Haifa 3200003, Israel. [6]Department of Cell and Developmental Biology, Sackler Faculty of Medicine, Tel Aviv University, Tel Aviv 6997801, Israel. [7]Poietis, Bioparc Bordeaux Métropole, Bordeaux 33600, France.
*These authors contributed equally to this work
‡These authors contributed equally to this work

§Authors for correspondence (dagmar.iber@bsse.ethz.ch; christophe.pierreux@uclouvain.be; francesca.spagnoli@kcl.ac.uk)

D.I., 0000-0001-8051-1035; C.E.P., 0000-0002-9647-2816; F.M.S., 0000-0001-7094-8188

DEVELOPMENT

subsequent differentiation, whereby cells at the 'tip' adopt an acinar differentiation program, whereas cells within the 'trunk' remain in a bipotent state and contribute to the ductal and endocrine cell lineages during further development (Fig. 1A′). Neighboring mesenchymal cells support this developmental process concomitantly with the formation of a vascular network (Angelo and Tremblay, 2018; Azizoglu and Cleaver, 2016;

Cozzitorto and Spagnoli, 2019; Golosow and Grobstein, 1962; Sakhneny et al., 2019; Seymour and Serup, 2019). Depletion of the mesenchyme impairs pancreatic epithelial growth, morphogenesis and differentiation of acinar and β-cells, suggesting a fundamental regulatory role for these cells throughout embryonic development (Attali et al., 2007; Cozzitorto et al., 2020; Esni et al., 2001; Harari et al., 2019; Landsman et al., 2011; Yung et al., 2019).
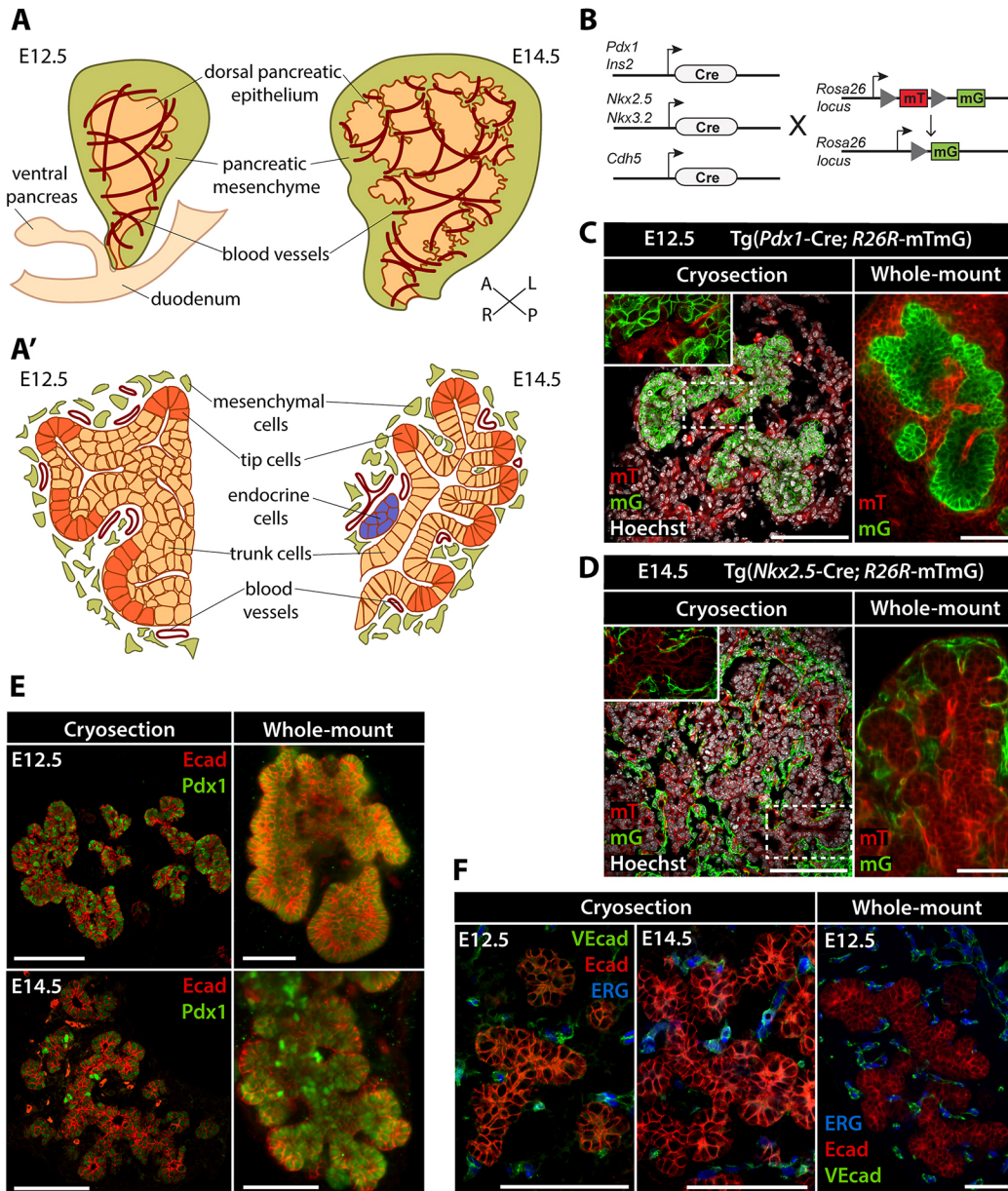

Fig. 1. Analysis of pancreatic morphogenesis using confocal microscope and LSFM. (A,A′) Schematics of the pancreatic epithelium, spleno-pancreatic mesenchyme, and developing vasculature in E12.5 and E14.5 mouse embryos in 3D (A) or transverse section (A′). Depiction of tissue architecture in the transverse section highlights the segregation of the pancreatic epithelium into domains of 'tip' and 'trunk' cells from E12.5 onwards. A, anterior; L, left; P, posterior; R, right. (B) Genetic strategy for labeling distinct mouse pancreatic, endothelial or mesenchymal cell populations. When not recombined, the Tg reporter construct mTmG results in the ubiquitous expression of a membrane-targeted tdTomato protein (mT). Cre-mediated recombination results in the excision of the mT expression cassette and expression of the membrane-targeted GFP (mG) in a tissue-specific fashion (Muzumdar et al., 2007). (C,D) IF detection of mG (green) and mT (red) in pancreatic tissue of E12.5 Tg(Pdx1-Cre, mTmG) embryos (C) or E14.5 Tg(Nkx2.5-Cre, mTmG) embryos (D). Pancreata analyzed as tissue sections by confocal microscopy (left) or as whole-mount preparations by LSFM (right) are shown side by side. In Pdx1-Cre Tg embryos (C), mG marks pancreatic epithelial cells. In Nkx2.5-Cre embryos (D), mG labels a subpopulation of mesenchymal cells in the spleno-pancreatic mesenchyme. Hoechst dye (gray) was used as nuclear counterstain on tissue sections. (E,F) Representative images of IF labeling of E12.5 and E14.5 pancreatic tissue. IF for Ecad (red; E,F) and Pdx1 (green; E) marks the pancreatic epithelium, whereas IF for ERG (blue; F) and VEcad (green; F) identifies endothelial cells surrounding the developing pancreas. Scale bars: 100 μm.

Similarly, endothelial cells influence different aspects of pancreatic tissue formation (Heymans et al., 2019; Jacquemin et al., 2006; Lammert et al., 2001, 2003; Magenheim et al., 2011; Pierreux et al., 2010).

Temporal aspects of pancreas development have been elucidated in great detail, also thanks to time-resolved studies in various vertebrate models, including zebrafish, frog, chick and mouse (Gittes, 2009; Larsen and Grapin-Botton, 2017; Zorn and Wells, 2009). These studies documented how and when early pancreatic progenitors commit to more specialized cell populations and how these processes can be recreated for *in vitro* differentiation and culture of pancreatic cell types. By contrast, spatial organization of the progenitor populations within the pancreas remains incompletely understood, because its embryonic development has been mainly studied in two-dimensions on histological sections. Recent advances in microscopy techniques, as well as optimized methods for clarification of whole-tissue specimens, have provided us with tools to study the pancreas in three dimensions at an unprecedented level of detail in the developing embryo (Chung et al., 2013; de Medeiros et al., 2016; Khairy and Keller, 2011; Richardson and Lichtman, 2015; Susaki et al., 2014; Wan et al., 2019). In particular, light-sheet microscopy has proven ideal for studying whole tissue samples in three dimensions as it combines excellent optical sectioning capabilities with fast image acquisition speed and reduced photoinduced damage to the tissue (de Medeiros et al., 2016; Khairy and Keller, 2011; Roostalu et al., 2020; Swoger et al., 2014; Wan et al., 2019).

Here, we applied light-sheet fluorescence microscopy (LSFM) to visualize the developing pancreas in 3D and to map tissue interactions at key time points during organ development. To this aim, we established protocols for tissue clarification and whole-mount immunofluorescence (WMIF) labeling of pancreatic tissue. We selected and validated transgenic mouse models and antibodies to visualize specific pancreatic epithelial, mesenchymal and endothelial cell populations and optimized light-sheet microscopy imaging protocols. In addition, we defined computational solutions for image analysis and quantification that enable detailed analysis of tissue composition and cell-cell interactions for the whole pancreas or the endocrine compartment. Lastly, we combined our data in an open source online repository (referred to as the Pancreas Embryonic Cell Atlas) to serve the scientific community by enabling further investigation of pancreas organogenesis and development of bioengineering solutions.

RESULTS
Establishing the experimental tools to analyze pancreatic morphogenesis using light-sheet microscopy

Despite significant advancements in light-sheet microscopy, protocols for WMIF labeling, tissue clarification and imaging have not yet been established for analysis of the developing pancreas and neighboring mesenchymal and endothelial tissues. Therefore, we started by testing antibodies and transgenic (Tg) mouse reporter strains for their suitability for 3D light-sheet microscopy of pancreatic tissue (Figs 1 and 2). Throughout the study, we compared data obtained by standard immunofluorescence labeling (IF) and confocal microscopy on pancreatic tissue sections with light-sheet microscopy images obtained from pancreata labeled by WMIF for endogenous proteins or fluorescent reporter expression.

To mark the location of specific cell populations in the mouse embryonic pancreas, we used different Cre-driver lines to induce the expression of fluorescent reporter genes in epithelial, mesenchymal

or endothelial progenitor cell populations (Figs 1B-D and 2). Reporter genes typically encode fluorescent proteins that can be visualized by detection of native fluorescence or immunolabeling with antibodies (Kretzschmar and Watt, 2012). For light-sheet microscopy and image segmentation, we chose the Tg(R26R-mTmG) [referred to as Tg(mTmG)] dual-fluorescent Cre reporter line, which is particularly suited for the visualization of cell-cell boundaries owing to the membrane localization of the two reporter proteins (Kretzschmar and Watt, 2012; Muzumdar et al., 2007; Snyder et al., 2013). The membrane-localized tdTomato (mT) is constitutively expressed in all cells of the mouse embryo; after Cre-mediated recombination, the expression of membrane-localized EGFP (mG) replaces the mT cassette in all *Cre*-expressing cells (Fig. 1B). We combined the Tg(mTmG) reporter line with five lineage-specific Cre Tg lines to label distinct cell types in the embryonic pancreas by the expression of mG (Fig. 1B). Specifically, we used the Tg(*Pdx1*-Cre) line to mark all cells of the pancreatic epithelium (Hingorani et al., 2003), the Tg(*Ins2*-Cre) line to mark insulin-expressing endocrine cells (Herrera et al., 1998), the Tg(*Cdh5*-Cre) line to mark endothelial cells (Chen et al., 2009), the Tg(*Nkx3.2*-Cre) and Tg(*Nkx2.5*-Cre) lines to label the entire spleno-pancreatic mesenchyme (Landsman et al., 2011; Verzi et al., 2009) and a subset of the mesenchymal cells surrounding the dorsal pancreas (Cozzitorto et al., 2020; Stanley et al., 2002), respectively.

Temporally, we focused our studies on stages E12.5 and E14.5 (Fig. 1A), key time points in mouse pancreatic morphogenesis and differentiation (Larsen and Grapin-Botton, 2017; Pan and Wright, 2011; Shih et al., 2013; Zhou et al., 2007). At E12.5, the pancreatic epithelium converts from a relatively smooth, multilayered epithelial bud into a highly branched epithelial monolayer (Fig. 1A′). At E14.5, the pancreatic epithelium further differentiates, and pancreatic progenitors within the branches undergo proximo-distal patterning to become increasingly lineage restricted (Fig. 1A′).

First, we optimized currently available protocols for the preparation of mouse embryonic samples for LSFM of the pancreas (see also Materials and Methods). For instance, to improve antibody penetration during WMIF labeling of embryonic pancreata, we extended the duration of the incubation steps with primary and secondary antibodies (Susaki et al., 2014). Moreover, to achieve complete tissue clarification, we modified the original CUBIC-based clarification protocols and the subsequent imaging setup (Susaki et al., 2014). Specifically, we subjected the WMIF-labeled pancreatic tissue to a prolonged two-step clarification procedure using CUBIC1 and CUBIC2 reagents, which resulted in optimal image quality (see Materials and Methods for details).

To assess the image quality and resolution of our new protocols, LSFM of whole-mount pancreatic tissue from E12.5 Tg(*Pdx1*-Cre; mTmG) and E14.5 Tg(*Nkx2.5*-Cre; mTmG) embryos was compared with standard IF labeling and confocal microscopy on pancreatic tissue sections (Fig. 1C,D). A 3D LSFM scan of E12.5 pancreas displayed primary branch structures composed of Pdx1$^+$/mG-labeled epithelial cells surrounded by mesenchymal and endothelial tissues (mT) (Fig. 1C, right) with resolution comparable to 2D immunolabeled sections (Fig. 1C, left). Similarly, at E14.5 the pancreatic epithelial cells (mT) as well as Nkx2.5-Cre-labeled mesenchymal cells (mG) were clearly visible using both imaging methods (Fig. 1D). Overall, these results indicate that our LSFM approach enables high-resolution imaging, comparable to conventional confocal microscopy approaches in 2D,
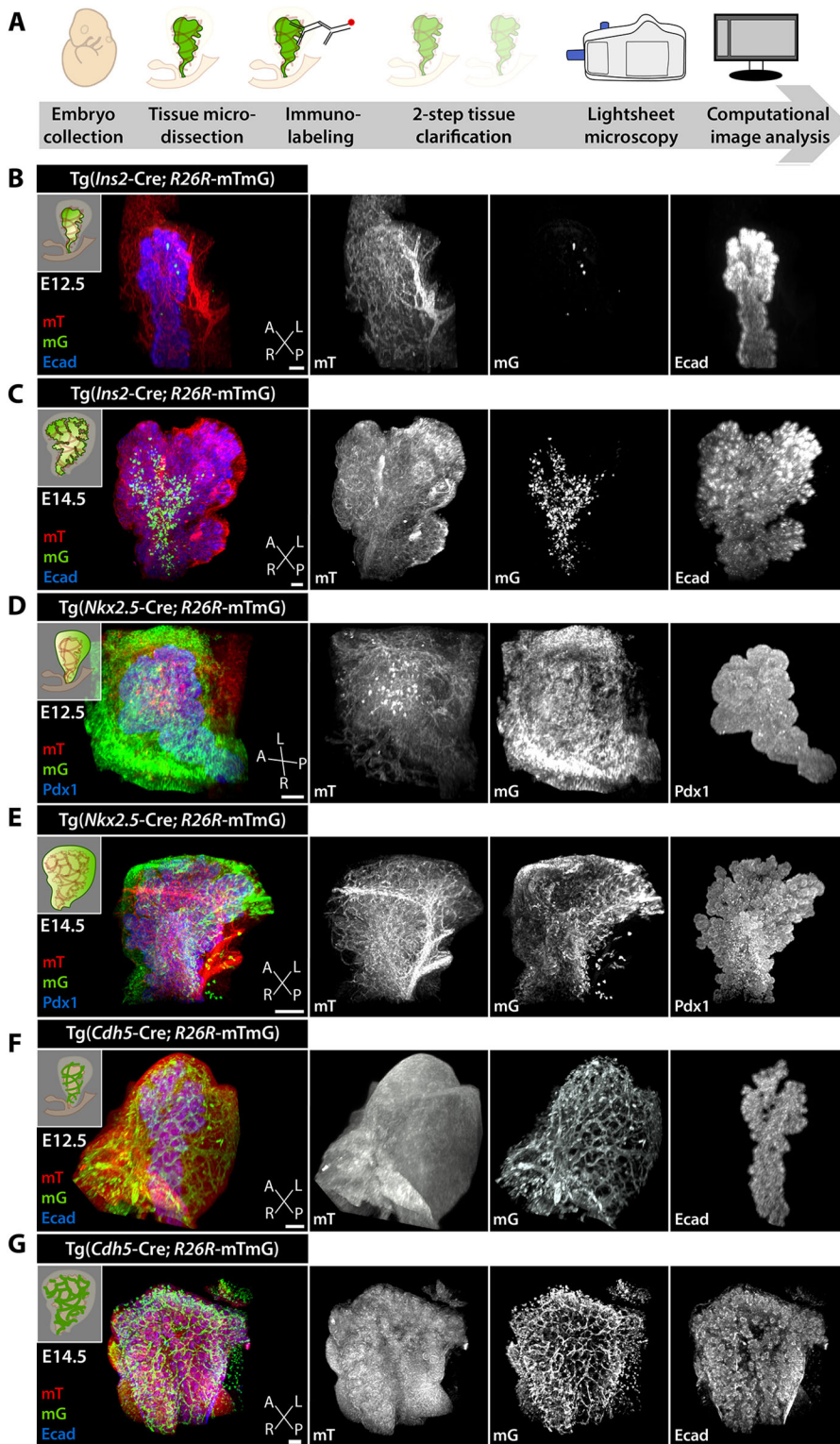
Fig. 2. 3D visualization of tissue interactions during pancreatic development using LSFM. (A) Schematic of the experimental setup for collection, visualization and imaging of pancreatic tissue from mouse embryos using LSFM. (B-G) Representative LSFM 3D images of pancreatic tissue from Tg mouse embryos at E12.5 (B,D,F) or E14.5 (C,E,G). Lineage-specific Cre induced mG expression in the indicated specific cell types. In *Ins2*-Cre; mTmG Tg embryos (B,C), mG marks insulin-expressing cells. In *Nkx2.5*-Cre; mTmG Tg embryos (D,E), mG labels a subset of mesenchymal cells in the spleno-pancreatic mesenchyme. In *Cdh5*-Cre; mTmG Tg embryos (F, G), mG marks endothelial cells. In addition to detection of mG and mT, samples were stained for Pdx1 (D,E; blue) or Ecad (B,C,F,G; blue) to visualize pancreatic epithelial cells. A, anterior; L, left; P, posterior; R, right. Scale bars: 100 μm.

but with the important advantage of preserving 3D tissue architecture and avoiding technical artifacts due to tissue freezing, embedding and/or sectioning.

Next, we explored the potential of combining the detection of lineage-specific fluorescent reporters with IF for endogenous proteins in whole-mount preparations to visualize specific cell populations. Antibodies against surface markers of epithelial [E-cadherin (hereafter Ecad; also known as Cdh1)] and endothelial cells [VE-cadherin (hereafter VEcad; also known as Cdh5)], as well as nuclear pancreatic [pancreatic and duodenal homeobox 1 (Pdx1)] and endothelial [ETS-related gene (ERG)] transcription factors were tested in parallel in conventional confocal microscopy and LSFM imaging approaches. Both approaches showed consistent results enabling visualization of endogenous proteins in addition to the mG- and mT-labeled cells (Fig. 1E,F).

3D rendering of the developing pancreas enables qualitative assessment of tissue architecture

The main morphogenetic events underlying primary and secondary branch formation in the pancreas occur between E12.5 and E14.5 in the mouse (Larsen and Grapin-Botton, 2017; Pan and Wright, 2011; Shih et al., 2013). So far, more attention has been paid to the intrinsic epithelial cell organization into defined branch shape and structure (Bankaitis et al., 2015; Hick et al., 2009; Kesavan et al., 2014, 2009; Petzold et al., 2013; Puri and Hebrok, 2007; Sznurkowska et al., 2018; Villasenor et al., 2010) than to the spatial organization of the different cell types, which surround the pancreatic branches. To fill this gap and capture the 3D structure of the whole organ, we acquired images of E12.5 and E14.5 whole-mount pancreata (Fig. 2). After image acquisition, the data were processed using ZEN and Imaris software (Fig. 2B-G) to generate 3D representations of the acquired images. We generated a set of high-resolution images from E12.5 and E14.5 pancreata, in which epithelial and mesenchymal (Fig. 2B-E) or epithelial and endothelial cells (Fig. 2F,G) were simultaneously marked in the same embryo. This dataset provided us with suitable material to analyze further the interactions between the pancreatic epithelium and surrounding tissues.

Using the 'Surface' and 'Spots' components in Imaris, we reconstructed the pancreatic epithelium, mesenchyme and its vascular network in three dimensions and performed different analyses on the obtained 3D surface renderings, such as quantification of blood vessel diameter and distribution of endothelial/mesenchymal cells around the pancreatic epithelium (Figs 3 and 4). When comparing 3D surface renderings of the epithelium at E12.5 and E14.5, we observed an increase in branching complexity with time that was accompanied by a more densely packed blood vessel network wrapping the epithelium (Fig. 3A,B) as well as closer contacts of the Nkx2.5-Cre$^+$ mesenchymal cells with the epithelium (Fig. 3C,D). Moreover, 3D surface renderings of the Nkx2.5-descendant mesenchymal population showed its preferential distribution along the left axis of the dorsal pancreatic epithelium (Fig. 3C,D), as previously reported by standard confocal image analysis (Cozzitorto et al., 2020).

LSFM imaging enables quantitative analysis of tissue organization during development

LSFM images are a source of qualitative but also quantitative information that complement 2D observations, inform on pancreas organogenesis, or generate image-driven hypotheses. For instance, 3D reconstruction of the VEcad$^+$ vascular network at E12.5 and E14.5 allowed us to measure the diameter of the blood vessels in spatial proximity to the pancreatic bud (up to 15 μm from the epithelial surface). We found a twofold increase in the average diameter of blood vessels closely associated with the pancreatic epithelium between E12.5 and E14.5 (Fig. 3E). These findings support the notion that a perfused and mature vascular network is established in the pancreas between E12.5 and E14.5, as previously suggested (Shah et al., 2011).

Additionally, we quantified the distribution of endothelial and Nkx2.5-Cre$^+$ mesenchymal cells with respect to their distance from the epithelial surface and analyzed its changes over time. 3D renderings of the pancreatic epithelium surface were based on Ecad (Fig. 4A) or Pdx1 (Fig. 4B) WMIF images, whereas the Imaris 'Spots' function enabled identification of endothelial or Nkx2.5-Cre$^+$ mesenchymal cells based on ERG (Fig. 4A) and mG (Fig. 4B) expression, respectively. We limited our analysis to endothelial and mesenchymal cells within a range of 15 μm from the epithelial

surface, as cells in proximity are likely to influence morphogenetic events of the underlying epithelium through paracrine signaling or physical constraint. Comparison of the distribution of endothelial and Nkx2.5-Cre$^+$ mesenchymal cells within the 15 μm radius highlighted a trend towards increased density of both cell populations in close proximity (0-7.5 μm) with the pancreatic epithelium as development progresses (Fig. 4C,D). By plotting the cumulative frequency distribution for endothelial and mesenchymal cells against their distance from the epithelium, we measured about 68% of endothelial and 51% of Nkx2.5-Cre$^+$ mesenchymal cells present within the first cell layer (about 0-7.5 μm) at E12.5 and 82% of endothelial and 66% of Nkx2.5-Cre$^+$ mesenchymal cells at E14.5 (Fig. 4E,F). Notably, we found no changes in cell density within epithelial and non-epithelial pancreatic tissue between E12.5 and E14.5 (Fig. S1A-C), ruling out the possibility that cell compaction may be responsible for an increase in heterologous cell-cell interactions.

To validate and expand the analysis of endothelial cell distribution in relation to the pancreatic epithelium, we analyzed serial IF-labeled tissue sections and segmented epithelial and endothelial cells using HALO software (Fig. 4G). Quantification of the percentage of endothelial cells within the first and second cell layer around the pancreatic epithelium documented about 61% of endothelial cells in direct contact with the epithelium at E12.5 and 75% at E14.5 (Fig. 4H), thereby corroborating the results obtained from 3D images (Fig. 4C,E). Interestingly, equivalent analysis of the vasculature around the stomach epithelium revealed significantly lower proportions of endothelial cells contacting the gastric epithelium at E12.5 and E14.5 (21% and 15%, respectively). These results suggest a tissue-specific vascularization pattern, whereby the pancreatic epithelium might require a closer interaction with a dense endothelial network to successfully undergo the morphological changes and differentiation processes that occur during these developmental stages. Overall, these analyses underscore previously underappreciated spatiotemporal changes in the composition and organization of the immediate pancreatic microenvironment and warrant further investigations.

3D image analyses allow precise quantification of cell type abundance

Numerous studies previously highlighted the importance of a finely tuned balance between epithelial, endothelial and mesenchymal cell types to allow pancreatic growth and morphogenesis. For instance, the presence of an excessive number of endothelial cells has been shown to impair pancreatic growth and limit branching morphogenesis (Magenheim et al., 2011; Sand et al., 2011) as well as to promote endocrine islet hyperplasia and reduce acinar differentiation (Lammert et al., 2001; Pierreux et al., 2010). By contrast, depletion of mesenchymal cells leads to severe pancreatic hypoplasia (Landsman et al., 2011). Therefore, establishing the relative abundance of epithelial, endothelial and mesenchymal cell populations during pancreatic development is crucial for ongoing efforts to bioengineer pancreatic tissues through co-culture or 3D bioprinting of heterologous cell populations.

To measure the relative abundance of the three cell types in the developing pancreas, we used 3D LSFM scans of E12.5 and E14.5 pancreata labeled for Ecad to mark epithelial cells and ERG to mark endothelial cells (Fig. 5A). DRAQ5 was used as nuclear counterstain. Using the 'Spots' function in Imaris, we quantified the number of epithelial (Ecad$^+$/ERG$^-$/DRAQ5$^+$), endothelial (Ecad$^-$/ERG$^+$/DRAQ5$^+$) and mesenchymal (Ecad$^-$/ERG$^-$/
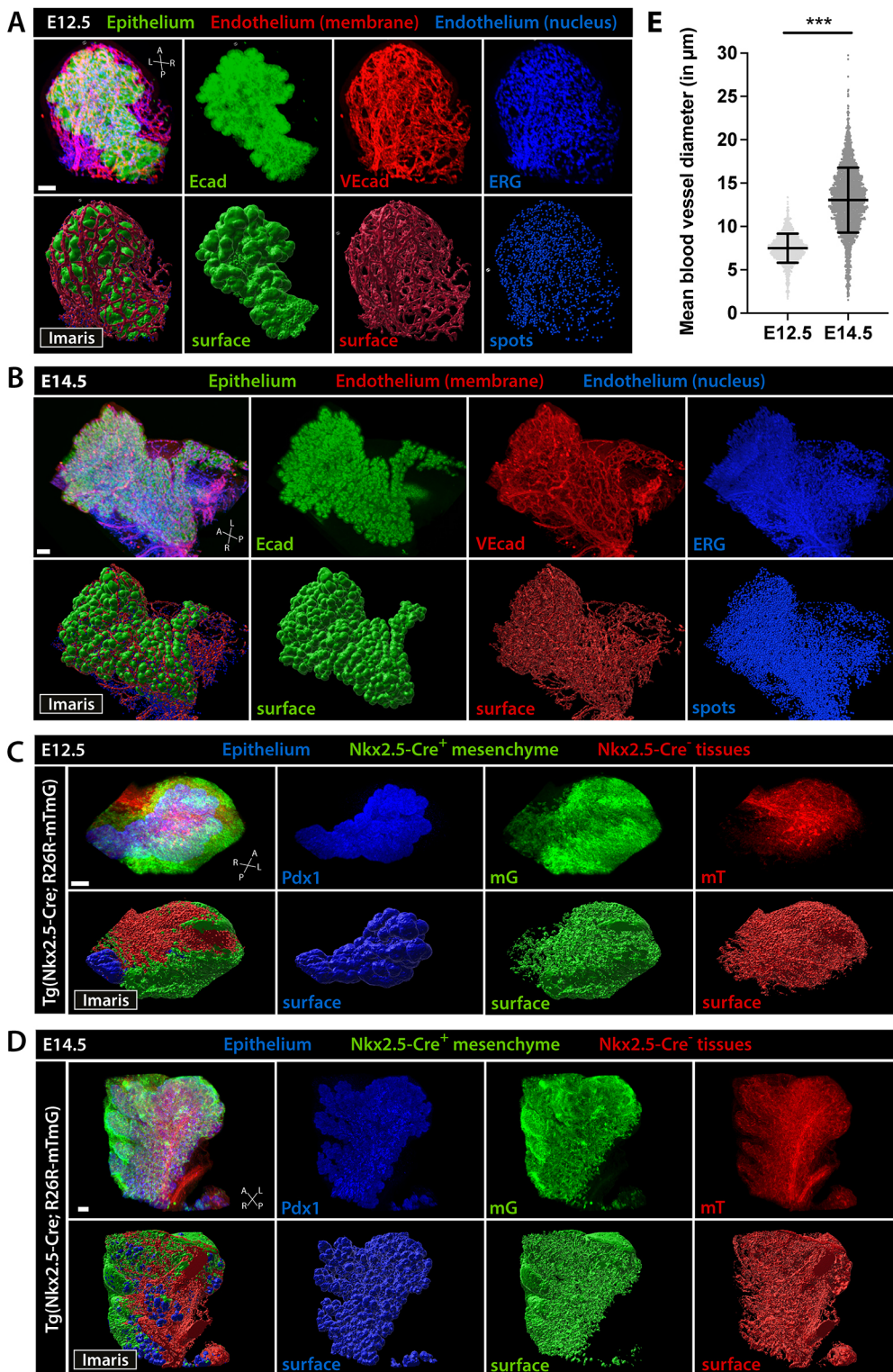
5

Fig. 3. 3D rendering of pancreatic tissue. (A-D) Representative LSFM 3D images (top) and Imaris surface renderings (bottom) of the developing pancreas from wild-type (A,B) or Tg(*Nkx2.5*-Cre; mTmG) (C,D) embryos at E12.5 and E14.5. WMIF for Ecad (A,B; green) or Pdx1 (C,D; blue) labels the pancreatic epithelium and for VEcad (red; A,B) or ERG (blue; C,D) marks the endothelium. mG (green; C,D) and mT (red; C,D) in Tg(*Nkx2.5*-Cre; mTmG) embryos mark the Nkx2.5-Cre[+] mesenchyme and Nkx2.5-Cre[−] tissues, respectively. 3D images and surface renderings are shown as merged (left) and individual channels (right). A, anterior; L, left; P, posterior; R, right. Scale bars: 100 µm. (E) Quantification of the mean diameters of blood vessels in close proximity (<15 µm) to the pancreatic epithelium at E12.5 (*n*=3) and E14.5 (*n*=2). Mann–Whitney test, ****P*<0.001. Data are mean±s.d.

DRAQ5^{+}) cells within a 15 µm distance from the epithelial surface, as in the cell distribution analysis (Fig. 4). We found that the proportions of epithelial (∼66%), endothelial (∼7%) and mesenchymal (∼27%) cells remain stable within this extended pancreatic region between E12.5 and E14.5 (Fig. 5C). It should be noted that in this analysis a mesenchymal cell identity was assigned based on the absence of epithelial and endothelial markers (Fig. 5), which does not exclude the presence of other cell types, such as neuronal, lymphatic or immune cells, in this fraction. However,

these cell populations are rare within the pancreatic tissue at E12.5 and E14.5 (Burris and Hebrok, 2007; Cozzitorto et al., 2020) (Fig. S1D), especially within the 15 µm radius from the epithelium, being therefore negligible in the calculation of relative cell abundance.

Next, we corroborated these results by assessing the relative abundance of the three cell populations on IF-labeled sections spanning the entire tissue and segmenting epithelial, endothelial and mesenchymal cells using the HALO software (Fig. 5B). Analogous
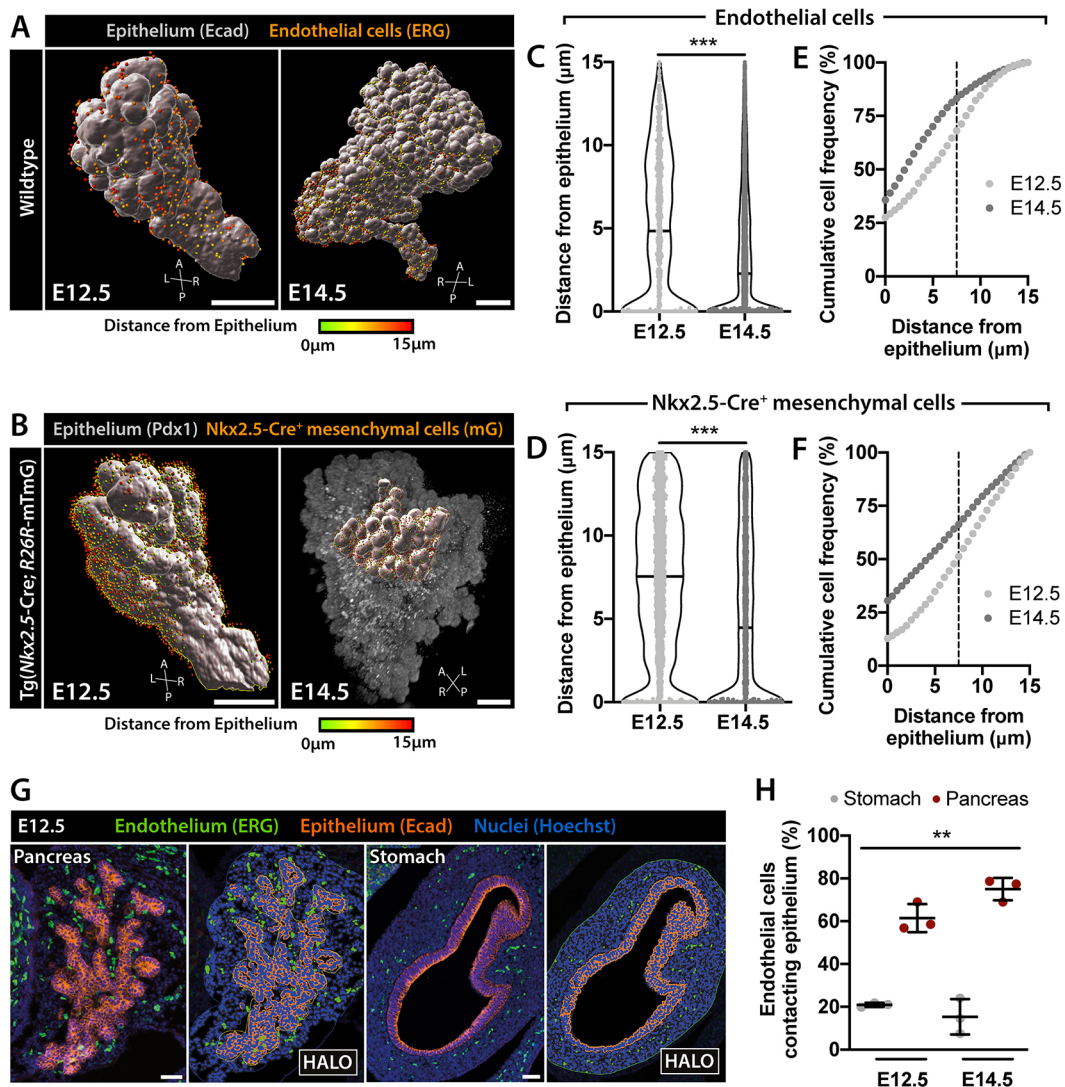
Fig. 4. Quantitative analysis of endothelial and mesenchymal cell distribution around the pancreatic epithelium. (A,B) 3D rendering of LSFM scans of E12.5 and E14.5 pancreas and surrounding tissues labeled with the indicated antibodies. Ecad+ (A) or Pdx1+ (B) pancreatic epithelial cells were rendered as surfaces (gray). ERG+ endothelial (spots, A) or Nkx2.5-Cre+ mesenchymal (spots, B) cells were identified using 'Spots' function in Imaris and color-coded based on their distance from the epithelium. Only endothelial or mesenchymal cells within a 15 µm distance from the epithelium were considered in the analysis. A, anterior; L, left; P, posterior; R, right. Scale bars: 200 µm. (C,D) Violin plots showing the distribution of endothelial (C) or Nkx2.5-Cre+ mesenchymal (D) cells around the pancreatic epithelium at E12.5 [n=799 cells (C); n=3350 cells (D)] and E14.5 [n=7817 cells (C); n=3359 cells (D)]. Mann–Whitney test, ***P<0.001. (E,F) Analysis of endothelial (E) or Nkx2.5-Cre+ mesenchymal (F) cell distance from pancreatic epithelium presented as cumulative frequency distribution. The percentage of endothelial (E) or Nkx2.5-Cre+ mesenchymal (F) cell population is plotted against the distance from the epithelium. Dashed vertical line indicates the 7.5 µm boundary, which corresponds approximately to the thickness of the first cell layer in direct contact with the epithelium. (G) Representative images of Ecad (orange) and ERG (green) IF labeling in E12.5 pancreas and stomach sections. Hoechst (blue) was used as nuclear counterstain. Scale bars: 50 µm. (H) Scatter plot showing quantification of endothelial cell distance from the pancreas or stomach epithelium at E12.5 (n=3) and E14.5 (n=3). Quantification was performed using HALO software. Data represents the number of endothelial cells localized within the first cell layer from the epithelium as a percentage of the total number of endothelial cells within a distance <15 µm from the pancreas or stomach. Kruskal–Wallis test, **P<0.001. Data are mean±s.d.

to our previous analysis, we restricted our analysis to tissues within a 15 µm range from the epithelium. We used a nuclear counterstain to mark all cells within the region of interest (ROI) in combination with antibodies against Ecad to mark epithelial and ERG to mark endothelial cells. The values in the proportions of epithelial (~56%), endothelial (~6%) and mesenchymal (~38%) cells remained constant between E12.5 and E14.5 (Fig. 5D). Notably, we observed only minor discrepancies in the percentages of epithelial (~66% versus ~56%) and mesenchymal cells (~27% versus ~38%) when comparing results obtained from 3D LSFM scans and 2D confocal images (Table 1). This is likely due to differences in cell segmentation between the Imaris and HALO

software used for the image analysis; by contrast, measurement of absolute cell numbers showed comparable results with both software (Fig. S1E).

In conclusion, we used 3D and 2D image analysis pipelines to assess the relative abundance of the three main cell types in the pancreatic tissue during development. Interestingly, our findings indicate that, despite profound morphological changes in tissue architecture between E12.5 and E14.5, the relative cell type composition in the pancreatic tissue does not change. Hence, an optimal ratio of epithelial (~60%) to endothelial (~6%) to mesenchymal (~34%) cells might be required to support pancreatic development.
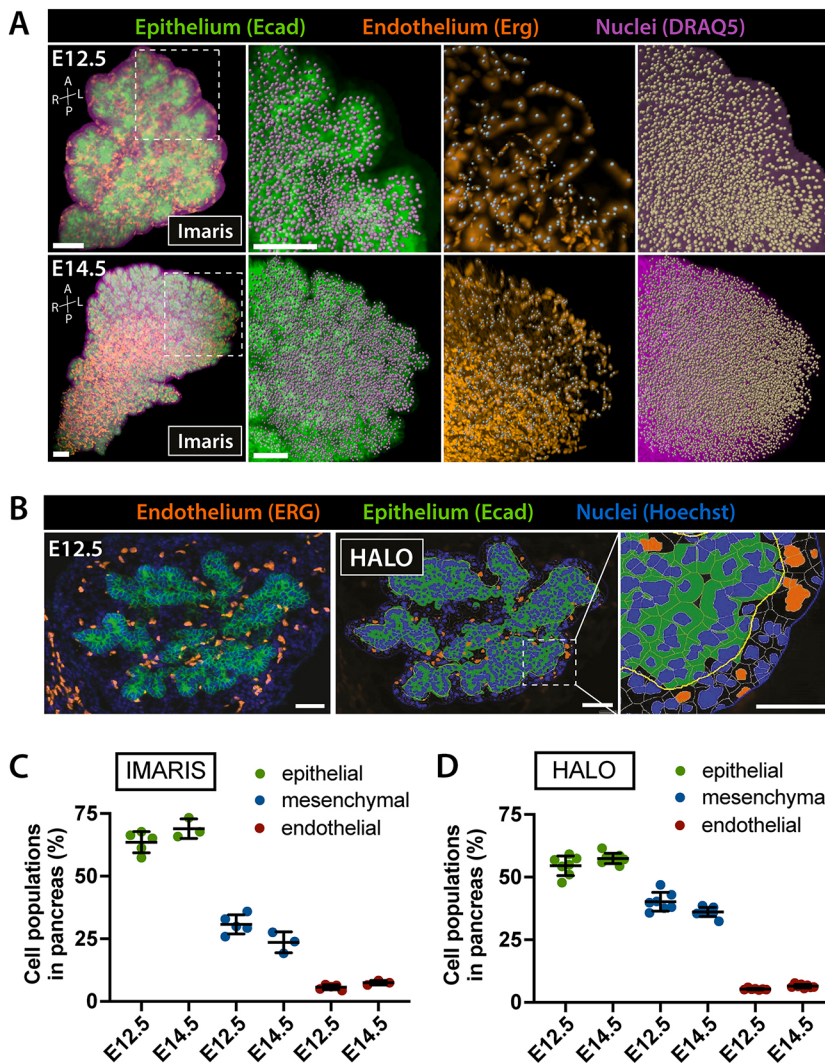
Fig. 5. Tissue segmentation of murine embryonic pancreas. (A) 3D representation of LSFM scans of E12.5 and E14.5 pancreas and surrounding tissues labeled with antibodies against Ecad (epithelial cells; green) and ERG (endothelial cells; orange). DRAQ5 was used as nuclear counterstain. The 'Spot detection' function in Imaris was used to identify all cells (based on DRAQ5), individual epithelial (Ecad$^+$) or endothelial cells (ERG$^+$) in the indicated boxed regions. Mesenchymal cells were identified as DRAQ5$^+$/Ecad$^-$/ERG$^-$. Analysis was restricted to surrounding tissue within 15 μm distance from the epithelial surface. Right-hand panels show higher magnification single-channel images of the boxed region. Scale bars: 100 μm. (B) Representative image of Ecad and ERG IF labeling of E12.5 pancreatic tissue sections (left). Hoechst was used as nuclear counterstain. Epithelial, endothelial and mesenchymal cells were segmented using HALO software (middle). Right-hand panel shows higher magnification of the boxed region. Mesenchymal cells were identified as Ecad$^-$/ERG$^-$/Hoechst$^+$. Scale bars: 50 μm (left and middle); 20 μm (right). (C,D) Scatter plots of the relative abundance of endothelial, epithelial and mesenchymal cells within a 15 μm radius of pancreatic tissue, shown as percentage of total cell numbers. Analysis of cell type fractions in C was performed using Imaris software on LSFM of whole-mount samples (A), whereas the analysis in D was performed using HALO software on confocal images of IF sections (B). No differences in cell fractions were detected between embryonic stages (E12.5 versus E14.5) or analysis pipelines (Imaris versus HALO). Kruskal–Wallis test, followed by Dunn's multiple comparisons test. Data are mean±s.d.

3D images allow visualization and quantification of the endocrine islet microenvironment

From E12.5 onward, endocrine progenitors start to appear within the bipotent trunk epithelium and, subsequently, differentiate into the five hormone-producing cell types that make up the islets of Langerhans in the adult pancreas (Pan and Wright, 2011). The development and maturation of hormone-producing cells depend on a combination of both intrinsic regulators and extrinsic cues from the surrounding tissues (Cozzitorto et al., 2020; Nikolova et al., 2006). Recent studies have highlighted a tight connection between endocrine cell differentiation and acquisition of islet architecture (Sharon et al., 2019). We reasoned that 3D LSFM imaging of the intact endocrine tissue might shed light on its architecture and

topological interactions with the vascular network and mesenchymal cells. Pancreatic tissue from wild-type embryos and newborns (P0) as well as from Tg(*Nkx2.5*-Cre; mTmG) embryos was subjected to WMIF labeling for endocrine (glucagon, insulin) and endothelial (VEcad) markers to visualize endocrine islet development (Figs 6 and 7). At E14.5, glucagon$^+$ cells were visible as small aggregates emerging from the Pdx1$^+$ epithelium; as development progressed, glucagon$^+$ clusters increased in size and occupied an outer position compared with Pdx1$^+$ or insulin$^+$ cells (Fig. 6; Fig. S2). These 3D structures are in line with the peninsular architecture model of islet formation (Sharon et al., 2019), whereby glucagon$^+$ α-cells bud out as units, forming a layer of cells that remain at the periphery of the peninsula, and are pushed by newly

Table 1. Proportion of endothelial, epithelial and mesenchymal cells in murine embryonic pancreas

	E12.5 (%)			E14.5 (%)		
	Endothelial	Epithelial	Mesenchymal	Endothelial	Epithelial	Mesenchymal
HALO segmentation*	5.3	54.5	40.2	6.5	57.4	36.1
IMARIS segmentation‡	5.6	63.6	30.8	7	69.3	23.7

*Percentage of epithelial, endothelial and mesenchymal cells quantified on regularly spaced sections (every 30 μm) spanning the entire pancreatic tissue at E12.5 (*n*=7) and E14.5 (*n*=8) from five independent litters at each stage.

‡Percentage of epithelial, endothelial and mesenchymal cells quantified on five areas of 300×300×300 μm of E12.5 (*n*=5) pancreata and three areas of 400×400×400 μm of E14.5 pancreata (*n*=3).
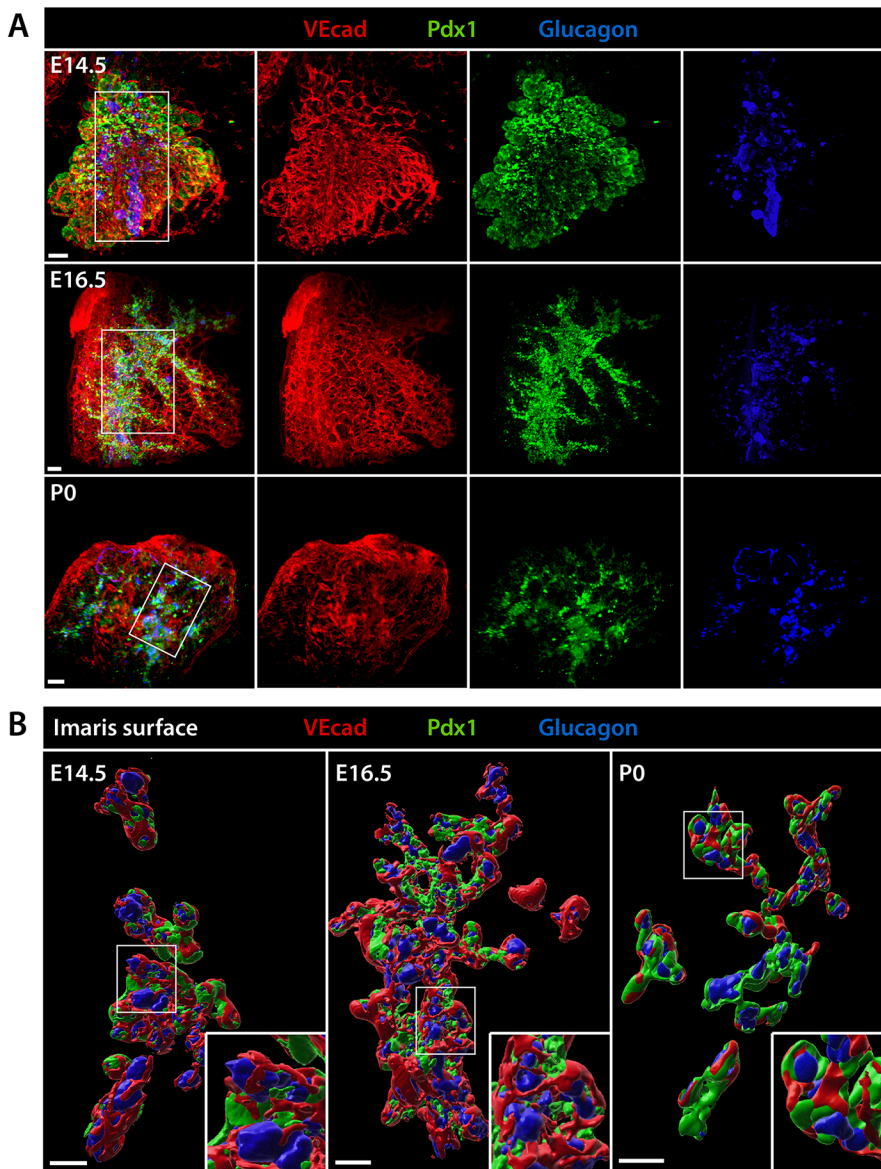
Fig. 6. 3D rendering of pancreatic tissue.
(A) Representative LSFM 3D images of the endocrine pancreas from wild-type embryos at E14.5, E16.5 and newborns at P0. WMIF for VEcad (red) marks the endothelium, glucagon (blue) labels the endocrine α-cells, Pdx1 (green) labels the pancreatic epithelium at E14.5 and becomes enriched in endocrine cells from E16.5 onward. 3D images are shown as merged (leftmost panels) and individual channels. (B) Surface renderings of the boxed area in A show glucagon$^+$ cells forming budding peninsular structures attached to the epithelial cords. Insets display the boxed area at higher magnification. Scale bars: 100 μm.

formed insulin$^+$ β-cells at the rear. Interestingly, we found that budding endocrine clusters were wrapped by endothelial (VEcad$^+$) cells, from the time of their early appearance (Fig. 6; Fig. S3). Tracking individual glucagon$^+$ cell clusters over successive LSFM z-slices showed that blood vessels were always present around developing peninsular structures, as if endocrine clusters budding was coordinated with the growth of blood vessels (Fig. S3).

Next, 3D LSFM scans of E14.5 and E16.5 wild-type or Tg(*Nkx2.5*-Cre; *R26R*-H2B-GFP) pancreas labeled with VEcad and glucagon were segmented to analyze and quantify the mesenchymal (GFP$^+$) and endothelial (VEcad$^+$) cells surrounding the endocrine clusters, as defined by peripheral glucagon$^+$ staining (Fig. 7A,B). We first focused on the vasculature and measured the diameter of VEcad$^+$ structures surrounding the endocrine clusters. The most frequent vascular structures found in proximity to the glucagon$^+$ cell surface had a diameter of approximately 8-12 μm, with the largest vessels displaying a diameter of 26 μm (Fig. 7C,D). Specifically, we found a higher relative frequency of small capillaries (<10 μm) in the close vicinity (0-15 μm) of the forming islets at both E14.5 and E16.5 stages, whereas the relative frequency of larger vessels (>12 μm) increased at a further

distance (0-50 μm) (Fig. 7C,D). Moreover, the vascular density increased as the pancreas developed and was found higher in close proximity (0-15 μm) to the endocrine clusters than at a distance (15-50 μm) (Fig. 7E). Similarly, we measured more mesenchymal cells present in the vicinity (0-15 μm) of the endocrine clusters at both stages, but, in contrast to the vasculature, the overall mesenchyme density decreased from E14.5 to E16.5 (Fig. 7F). Altogether, these data suggest (1) coordinated development of endocrine peninsula with vascular blood vessels, and (2) remodeling of the vasculature along with endocrine islet formation, with small vessels sprouting in close contact with islet cells.

The Pancreas Embryonic Cell Atlas as an open access data repository
All 3D LSFM images visualizing the three main cell types (epithelium, endothelium and mesenchyme) of the murine embryonic pancreas have been annotated and deposited on the open-source database openBIS (open Biology Information System) (https://openbis.ch/) to start building a Pancreas Embryonic Cell Atlas (Table S1). We built a customized data-management platform
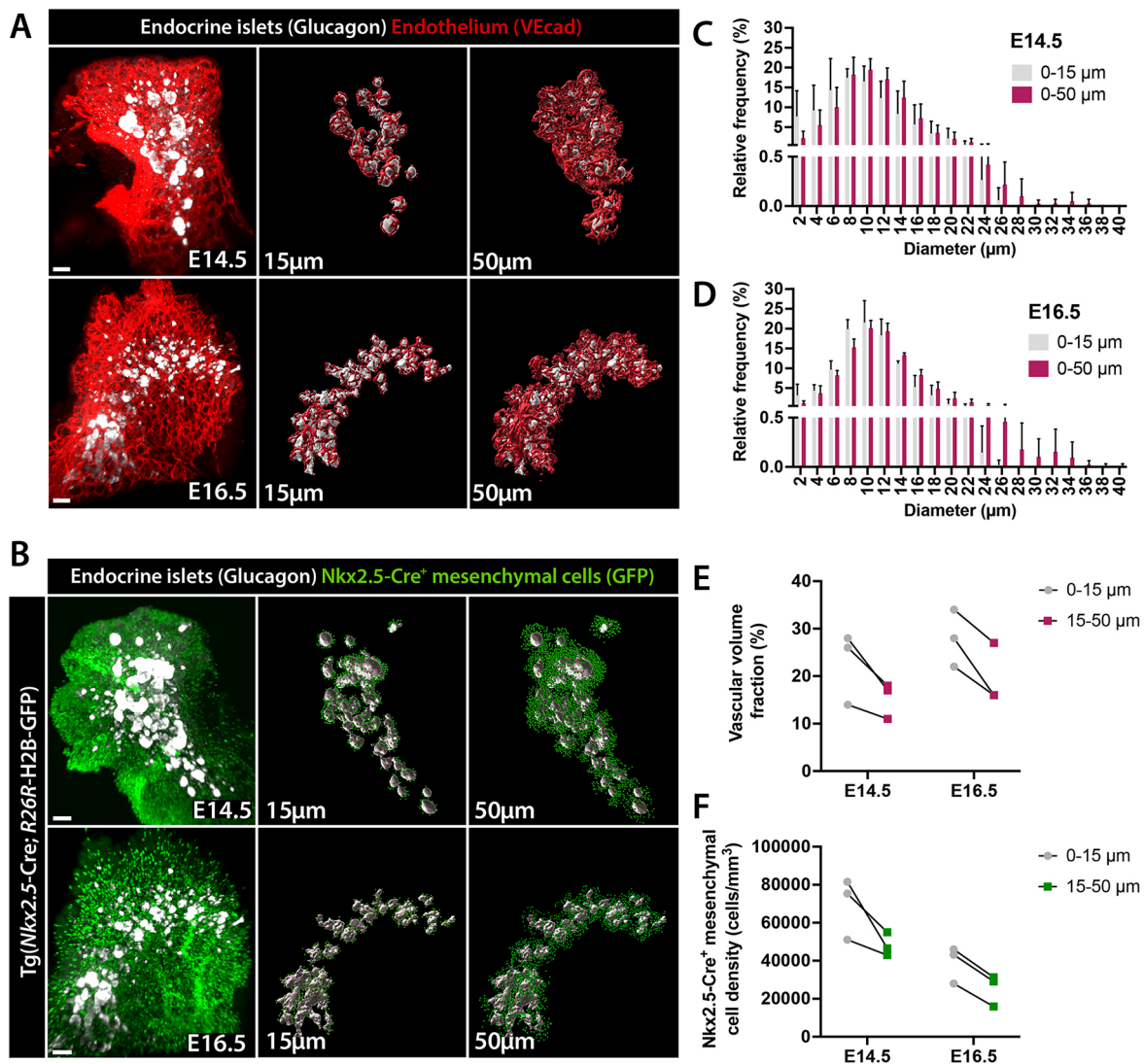
Fig. 7. Quantitative analysis of endothelial and mesenchymal cell density around the pancreatic endocrine clusters. (A,B) 3D rendering of LSFM scans of E14.5 and E16.5 pancreata from wild-type or Tg(Nkx2.5-Cre; R26R-H2B-GFP) embryos. WMIF for glucagon (white) labels the endocrine α-cells, VEcad (red) marks the endothelium (A), and Nkx2.5-Cre+ mesenchymal cells are GFP+ (green) (B). Central and right panels show endocrine clusters composed of at least eight glucagon+ cells (3D rendering volume >67,700 μm³) rendered as surfaces (white) for quantitative analyses. Endothelial and mesenchymal cells within the close (up to 15 μm; central panels) and distant (up to 50 μm, right panels) microenvironment from the endocrine clusters were considered in quantitative analyses. Scale bars: 100 μm. (C,D) Vascular structure diameter distribution (relative frequency as percentage) in the microenvironment surrounding the endocrine clusters at E14.5 (n=3) (C) and E16.5 (n=3) (D). Data are mean±s.d. (E) Scatter plots showing the vascular volume fraction measurement at a distance of 0-15 μm and 15-50 μm from the endocrine clusters at E14.5 and E16.5. The vascular volume fraction was used as proxy for the vascular density, shown as ratio between the volume of the VEcad+ surface and the volume of the analyzed area (0-15 or 15-50 μm away from glucagon+ surface). (F) Scatter plots showing the mesenchymal density (Nkx2.5-GFP+ cells) in the microenvironment surrounding the endocrine clusters (glucagon+) at E14.5 and E16.5.

and all image data have been made available on the data management platform openBIS (https://openbis-pancreas-atlas. ethz.ch/). So far, 66 LSFM scans have been made publicly available in our data repository openBIS in the following formats: tiff (raw microscopy data), ims (proprietary format of Imaris containing microscopy images and surfaces with tissue shapes), wrl (tissue shapes exported separately), png (overview of the sample). Each image collection comprises a context-specific group of images and annotations, including developmental stage, mouse genotype, mouse background, segmented tissue, antibodies and conjugated fluorescent dyes (450 nm/488 nm/594 nm/647 nm), laboratory of origin, site of imaging and comments. See Materials and Methods and Fig. S4 for a description of how to access the data.

DISCUSSION

Spatial information on the interaction of pancreatic progenitor cell types with surrounding tissues is essential for the full comprehension of basic concepts governing pancreas development *in vivo*, but also for devising strategies for the *in vitro* generation of transplantable pancreatic tissue for regenerative therapies. To date, spatial information on pancreas development has mostly relied on 2D histological sections or *in silico* reconstructions (Bankaitis et al., 2015; Bhushan et al., 2001; Heymans et al., 2019; Kesavan et al., 2014, 2009; Mamidi et al., 2018; Villasenor et al., 2010). Previous studies of whole-mount pancreatic tissue have provided excellent information on the gross morphology of the epithelium (Fowler et al., 2018; Jørgensen et al., 2007; Kesavan et al., 2009; Petzold et al., 2013; Sznurkowska et al., 2018; Villasenor et al., 2010),

but limited information on contacts and interactions with neighboring tissues. Here, we have established tools and protocols for WMIF labeling, tissue clarification, and light-sheet imaging of the developing pancreas and exemplified pipelines to utilize these data for the study of pancreatic organ development in the mouse, with a focus on the developing islets.

Currently, heterologous tissue interactions, such as epithelial-mesenchymal or epithelial-endothelial crosstalk during pancreas development, have gained a lot of attention because of their essential role in pancreatic cell differentiation (Attali et al., 2007; Azizoglu and Cleaver, 2016; Cozzitorto et al., 2020; Heymans et al., 2019; Landsman et al., 2011; Pierreux et al., 2010; Sakhneny et al., 2019; Seymour and Serup, 2019; Yung et al., 2019). As a proof of concept, here we exemplified how to extract information on the 3D tissue architecture as well as the relative position of epithelial, mesenchymal and endothelial cells from LSFM images of the developing pancreas. These data provide us with the ability to visualize the intimate interaction between epithelial cells and Nkx2.5$^+$ mesenchymal cells, which contribute to the proper development of the endocrine pancreas (Cozzitorto et al., 2020). Moreover, our LSFM images enabled the visualization of endocrine cluster formation within their immediate microenvironment. Our results support the suggestion that endocrine cells bud out of the trunk epithelium, as peninsular structures (Sharon et al., 2019), without migrating away from the epithelium. Interestingly, on their route to becoming mature islet structures, endocrine cells are constantly and increasingly in contact with endothelial cells forming small vessels, whereas the interactions with mesenchymal cells decrease over time. These findings suggest distinct cell-cell interaction requirements for early endocrine cell specification and for late differentiation/maturation. The reduction of Nkx2.5$^+$ mesenchymal cells around the developing islets could be due to reduced proliferation rate in an expanding organ and/or to differentiation into other lineages, such as pericytes (Sakhneny et al., 2019).

Notably, our results suggest a tissue-specific vascularization pattern, whereby the embryonic pancreatic epithelium requires a closer interaction with a dense endothelial network compared with the neighboring stomach. This different pattern in epithelial-endothelial cell interaction could be due to differences in the architecture of the two tissues, with the pancreas being a branching epithelium with more complex folding than the stomach. Another plausible explanation could be related to the different organ functions. The stomach is a glandular epithelium with mostly an exocrine function, whereas the pancreas is an amphicrine gland with an endocrine function and, therefore, requires a dense vascular network in contact with endocrine cells for collecting hormones from the islets (Gittes, 2009; Pan and Wright, 2011). Alternatively, the difference in epithelial-endothelial cell interactions could be due to the different expression of the angiogenic factor Vegfa. Indeed, starting from E14.5, *Vegfa* expression is higher in the trunk and branches of the pancreas compared with the stomach epithelium (Pierreux et al., 2010). This angiogenic signal might promote the recruitment and expansion of endothelial cells around the pancreatic epithelium, resulting in more intimate epithelial-endothelial contacts.

We have provided access to our acquired dataset through the Pancreas Embryonic Cell Atlas, an open source data repository (Fig. S4). So far, 3D LSFM-based analyses of the mouse embryonic pancreas together with its neighboring mesenchymal and endothelial tissues have not been reported. Thus, the Pancreas Embryonic Cell Atlas will provide the scientific community with a valuable source of data for future investigation. Similar to other open source data repositories, such as the human 'Pancreatlas' (https://www.pancreatlas.org/) (Saunders et al., 2020), we envision the Pancreas Embryonic Cell Atlas as a dynamic platform that will evolve with continued input from us and others. Foremost, the collection of raw data deposited in the Pancreas Embryonic Cell Atlas will help the scientific community to develop and test novel hypotheses on tissue interactions that guide pancreatic differentiation and morphogenesis. Also, we provide datasets of already rendered surfaces (shown in Fig. 3) that can be viewed using the free Imaris Viewer software, ImageJ and QuPath (Fig. S5), and do not require access to commercial software or high-performance computing. Finally, we envision that Pancreas Embryonic Cell Atlas image collections will identify collaborations also outside the pancreas field and lay the foundation of interdisciplinary work that integrates cellular-resolution data within the context of whole-organ architecture.

MATERIALS AND METHODS
Animal experimentation
The following transgenic mouse lines were used: Tg(*Pdx1*-Cre) (Hingorani et al., 2003), Tg(*Nkx3.2*-Cre) (Verzi et al., 2009), Tg(*Nkx2.5*-Cre) (Stanley et al., 2002), Tg(*Ins2*-Cre) (Herrera et al., 1998), Tg(*Cdh5*-Cre) (Chen et al., 2009) and Tg(*R26R*-mTmG) (Muzumdar et al., 2007). All mouse strains were on a C57BL/6 genetic background and kept under standard housing conditions. All procedures relating to animal care and treatment conformed to the Institutional Animal Care and Research Advisory Committee and local authorities (PPL PP6073640, Home Office, UK; University Animal Welfare Committee UCLouvain 2016/UCL/MD/005 and 2020/UCL/MD/011; Veterinary Office of Canton Basel-Stadt, Switzerland; Tel Aviv University Committee on Animal Research). For timed mating, male and female mice were placed into a breeding cage overnight and plug check was performed daily. The presence of a vaginal plug in the morning was noted as E0.5. Embryos at E12.5, E14.5, E16.5 and E18.5 and newborns at P0 were collected and dissected under a stereomicroscope.

Immunofluorescence labeling of mouse tissue sections
After dissection, embryos were fixed in 4% paraformaldehyde (PFA) in PBS overnight at 4°C. For generation of paraffin sections, fixed embryonic tissue was embedded in paraffin using a Tissue-Tek VIP-6 (Sakura). For generation of cryosections, fixed embryonic tissue was equilibrated overnight in 20% sucrose solution and embedded in O.C.T. compound (Tissue-Tek, Sakura). Paraffin sections and cryosections were cut at 7 µm and 10 µm thickness, respectively. Prior to immunolabeling, paraffin sections were deparaffinized with xylene for 10 min and rehydrated. If required, antigen retrieval was performed using citrate buffer [0.01 M citric acid and 0.05% Tween 20 (pH 6.0)] for 10 min in the microwave (750 W). Next, tissue sections were incubated in TSA (Perkin Elmer) blocking buffer for 1 h at room temperature followed by overnight treatment at 4°C with primary antibodies at the appropriate dilution (Table S2). Next, tissue sections were incubated for 1 h at room temperature with Hoechst 33342 nuclear counterstain at a concentration of 250 ng/ml and secondary antibodies at the appropriate dilution (Table S2). Slides were mounted with Dako fluorescence mounting medium and imaged on a Zeiss LSM 700 confocal microscope using a 25× or 40× oil immersion objective.

Immunofluorescence labeling of whole-mount mouse tissue
Embryos were collected at E12.5, E14.5, E16.5 and E18.5 and newborns at P0, and the trunk region posterior to the forelimbs and anterior to the hindlimbs was dissected. The duodenum, stomach, dorsal and ventral pancreas as well as associated mesenchymal tissues were dissected and harvested as a continuous unit. Optionally, to simplify the image acquisition of the pancreas at E14.5, the stomach was removed. The dissected tissues were fixed in 4% PFA for 1-2 h at room temperature (at E12.5-E16.5) or overnight at 4°C for later stages and then extensively washed in 1× PBS. Subsequently, samples were placed in blocking solution [3% donkey serum

(DS), 0.1% (at E12.5) or 0.5% (at E14.5) Triton X-100 in 1× PBS] for 32 h at 4°C and afterwards incubated with primary antibodies in blocking solution at the appropriate dilution for 48 h at 4°C (see Table S2). After washes in freshly prepared 1× PBS with 0.1% Triton X-100 solution (at least three times, 5 min each, followed by an overnight washing step at 4°C), the samples were incubated with secondary antibodies appropriately diluted (see Table S2) together with Hoechst 33342 nuclear counterstain (250 ng/ml) in blocking solution for 32 h at 4°C. After extensive washing steps in 1× PBS with 0.1% Triton X-100 (as above), the samples were transferred into PBS and stored at 4°C until tissue clarification.

Tissue clarification

Pancreatic tissue was cleared in freshly prepared CUBIC1 [25% wt/vol urea, 25% wt/vol N,N,N′,N′-tetrakis(2-hydroxypropyl) ethylenediamine, 15% wt/vol Triton X-100, in dH$_2$O] and CUBIC2 (50% wt/vol sucrose, 25% wt/vol urea, 10% wt/vol 2,20,20′-nitrilotriethanol, 0.1% vol/vol Triton X-100, in dH$_2$O) solutions as previously described (Susaki et al., 2014).

The clarification protocol was adapted according to the mounting procedure used for light-sheet microscopy. If to be glued to a supportive holder, the sample was transferred into a glass vial containing 2 ml CUBIC1 solution and incubated for 3 weeks at room temperature on a rotational shaker in the dark. The tissue was then transferred into a new glass vial containing 2 ml of CUBIC2 solution, without carrying over any CUBIC1 solution, and incubated for 1 week at room temperature on a rotational shaker in the dark.

For agarose embedding, the sample was immersed in CUBIC1 at 37°C for 3 days in plastic Petri dishes or 4-well plates on a rotational shaker, then washed in PBS for 1 day at 4°C and transferred in CUBIC2 at room temperature for 3 weeks with solution changed every 3-5 days. During the PBS washing step, samples were again incubated with Hoechst 33342 nuclear counterstain (250 ng/ml). Both CUBIC1 and CUBIC2 incubation steps were preceded by an intermediate 1:2 dilution step of the respective solution of 24 h duration.

Sample mounting and light-sheet microscopy

Samples were glued to a 1 ml syringe supportive holder using all-purpose super glue. The syringe was then inserted into the syringe holder provided with the Zeiss Z1 light-sheet microscope. Specifically, the clarified tissue was retrieved from the CUBIC2 solution by removing as much solution as possible using either a pipette or paper wipes and glued to the tip of the syringe. To avoid interference with pancreatic tissue during imaging, the sample was glued on the stomach or duodenum. After 1 min, the sample holder was inserted into the microscope for image acquisition. Alternatively, for agarose mounting, the samples were embedded in a glass capillary, provided by Zeiss, filled with 2% low-melting point agarose solution. Afterwards, the solidified agarose cylinders containing the samples were immersed in CUBIC2 for 48 h to clear the agarose. Samples were then imaged with the Zeiss Z1 light sheet microscope using 20× acquisition and 10× illumination lenses.

Image analysis and cell segmentation

Imaris (Bitplane Oxford Instruments, version 9.5.1) software packages, including Imaris XT, Imaris Filament Tracer and Imaris Measurement Pro with IPSS and Statistics features, were used to segment the 3D images obtained from the light-sheet microscope. Volumes of the different cell populations in the developing pancreas were created using the 'Surface creation' module on the epithelial [E-cadherin (Ecad) or Pdx1 labeling], the endocrine [glucagon or insulin labeling], the endothelial [VE-cadherin (VEcad) labeling] and the Nkx2.5-Cre$^+$ mesenchymal populations.

For the analysis around endocrine clusters, we filtered out 3D rendering glucagon$^+$ surfaces with a volume smaller than 67.700 μm^3. Nuclei of endothelial and Nkx2.5-Cre$^+$ mesenchymal cells were reconstructed using the 'Spots creation' module and used as the center of the cell, based on the endothelial ERG signal and the signal of Nkx2.5-Cre;R26R-H2B-GFP- or the inverted signal of the Nkx2.5-Cre;R26R-mTmG-labeled mesenchymal cells (GFP or mG), respectively.

The mean vascular diameter was computed using the 'Filament tracer' extension on the VEcad labeling surrounding the epithelium bud and the

glucagon clusters within a distance of 15 μm and 50 μm. The mean diameter of each vascular segment between two junctions was extracted with the 'Measurement Pro' Extension package. The distribution of endothelial and *Nkx2.5*-expressing mesenchymal cells in the vicinity of the pancreatic bud was performed using the reconstructed volume of the epithelial cells and the spots generated for the endothelial and Nkx2.5-Cre$^+$ mesenchymal cells. Using the feature 'Shortest distance', the distance of each endothelial or Nkx2.5-Cre$^+$ mesenchymal cells from the epithelial surface was extracted. Because of the complex morphology of the pancreas with its multiple branches, some endothelial and Nkx2.5$^+$ cells appeared to be included in the epithelium volume. These cells were actually located in spaces between pancreatic branches and were considered at a distance of 0 μm, as they were in direct contact with epithelial cells.

To segment pancreatic tissue into single cells for cell type quantification, LSFM scans of pancreata labeled with antibodies against Ecad and ERG and DRAQ5 nuclear counterstain were analyzed at defined ROIs [300×300×300 μm (E12.5 pancreata) or 400×400×400 μm (E14.5 pancreata)]. Before proceeding with the segmentation, the Ecad membrane signal was subtracted from the DRAQ5 signal to obtain a sharper delineation of the nuclei. Additionally, the Ecad signal was blurred with a 'Gaussian filter' and inverted to obtain a filled cell signal with dark membranes. This multi-step image processing allowed us to identify three distinct types of 'Spots' in Imaris: one for epithelial cells based on the inverted Ecad signal; one for endothelial cells based on the ERG nuclear signal; one for all nuclei based on the DRAQ5 signal (identification settings for all were set to an *xy* diameter of 5 μm and a *z* diameter of 7 μm). To restrain the segmentation analysis to the epithelial bud and tissues in its immediate vicinity, an epithelial surface was created, as described above. Then, a filtering step was applied to exclude all nuclei and endothelial spots found at a distance greater than 15 μm from the epithelial surface. Next, an additional filtering step was applied to remove undesirable spots, such as multiple spots found in larger cells. Finally, the whole-organ segmentation process was verified by extracting virtual 2D sections of the fluorescence signals and their respective spot signals and by applying manual correction where necessary.

The image analysis software HALO (Indica Labs, v3.0.311.317) was used to segment images from tissue sections of E12.5 and E14.5 pancreatic and gastric tissue IF-labeled with Ecad and ERG antibodies and Hoechst nuclear counterstain. First, the area of interest was defined by manually delineating the pancreatic epithelium as well as the surrounding tissues within a distance of approximately 15 μm (about two cell layers) from the epithelium. The CytoNuclear FL v1.4 Algorithm was applied to segment the tissue into individual cells. This algorithm segments the nuclei based on Hoechst staining and further identifies distinct cell types based on the fluorochrome detected in the segmented area, i.e. Ecad marking epithelial cells and ERG marking endothelial cells. To quantify the distribution of endothelial cells around the pancreatic or gastric epithelium, the *xy* coordinates for endothelial and epithelial cells were extracted from the segmented images. Using R software, the number of endothelial cells in direct contact with the epithelium (0-7.5 μm distance from the epithelium) and within a 15 μm distance from the epithelium was computed. The relative abundance of epithelial, endothelial and mesenchymal cells was determined by quantifying the number of each cell type on regularly spaced sections (every 30 μm) spanning the entire pancreatic tissue (Gonay et al., 2021). Examples of visualization and quantitative analysis of LSFM 3D images using open-source software, such as ImageJ (3D Viewer plugin) and QuPath, are shown in Fig. S5.

Pancreas Embryonic Cell Atlas and browsing features

The images are stored on the data management platform openBIS (https://openbis.ch/). For repository access, first please contact the PAN3DP consortium (https://www.pan3dp-project.eu/ or pan3dp@kcl.ac.uk) to be granted guest access to the platform and then visit https://openbis-pancreas-atlas.ethz.ch/. The collections are accessible within the 'PAN3DP' space in the project called 'PANCREAS_ATLAS'. Each collection corresponds to one developmental stage. Within each collection, the objects correspond to specific genotypes, i.e. transgenic mouse lines. Each object contains individual samples, i.e. the image datasets. For a schematic representation of

data organization in the repository, see Fig. S4. Within each sample, images in all different formats can be retrieved using advanced filter commands and downloaded separately or collectively. To access the filters, go to the 'Utilities' section of the navigation menu (left side of the webpage) and click 'Advanced Search'. Set the 'Search For' box to 'Dataset' and insert the chosen filtering criteria. The data will be displayed in the 'Results' section and can be quickly accessed for viewing and download. The information displayed in the 'Results' table can be adapted according to individual needs using the 'Columns' drop-down menu.

For the most informative overview on the 3D architecture of the pancreas, it is recommended to view the surfaces combined with the multi-channel microscope images in the Imaris proprietary format (.ims) using the free Imaris Viewer (https://imaris.oxinst.com/imaris-viewer). To perform further modification on the data, the commercial version of Bitplane Imaris software is required. The raw .tiff files can be opened with open source software such as ImageJ or Fiji. The surface files in .wrl format can be opened using 3D mesh processing software, such as MeshLab.

Competing interests
The authors declare no competing or financial interests.

Author contributions
Conceptualization: L.G., A. Sapala, D.W., F.G., S.L., L.L., D.I., C.E.P., F.M.S.; Methodology: L.G., A. Sapala, D.W., M.M.; Software: A. Sapala, L.G., L. Schaumann, H.F.G., L.C.; Validation: L.G., A. Sapala, D.W., M.M., J.-F.D., S.E., A. Schonblum, L. Sakhneny, C.L.; Investigation: L.G., D.W., A. Salowka; Resources: L.L., D.I., C.E.P., F.M.S.; Writing - original draft: L.G., A. Sapala, D.W., C.E.P., D.I., F.M.S.; Writing - review & editing: L.G., D.W., L.L., C.E.P., F.M.S.; Supervision: D.I., C.E.P., F.M.S.; Funding acquisition: F.G., S.L., L.L., D.I., C.E.P., F.M.S.

Peer review history
The peer review history is available online at https://journals.biologists.com/dev/article-lookup/doi/10.1242/dev.199655.

References

Angelo, J. R. and Tremblay, K. D. (2018). Identification and fate mapping of the pancreatic mesenchyme. *Dev. Biol.* **435**, 15-25. doi:10.1016/j.ydbio.2018.01.003

Attali, M., Stetsyuk, V., Basmaciogullari, A., Aiello, V., Zanta-Boussif, M. A., Duvillie, B. and Scharfmann, R. (2007). Control of β-cell differentiation by the pancreatic mesenchyme. *Diabetes* **56**, 1248-1258. doi:10.2337/db06-1307

Azizoglu, D. B. and Cleaver, O. (2016). Blood vessel crosstalk during organogenesis-focus on pancreas and endothelial cells. *Wiley Interdiscip. Rev. Dev. Biol.* **5**, 598-617. doi:10.1002/wdev.240

Bankaitis, E. D., Bechard, M. E. and Wright, C. V. E. (2015). Feedback control of growth, differentiation, and morphogenesis of pancreatic endocrine progenitors in an epithelial plexus niche. *Genes Dev.* **29**, 2203-2216. doi:10.1101/gad.267914.115

Bhushan, A., Itoh, N., Kato, S., Thiery, J. P., Czernichow, P., Bellusci, S. and Scharfmann, R. (2001). Fgf10 is essential for maintaining the proliferative capacity of epithelial progenitor cells during early pancreatic organogenesis. *Development (Cambridge, England)* **128**, 5109-5117. doi:10.1242/dev.128.24.5109

Bulanova, E. A., Koudan, E. V., Degosserie, J., Heymans, C., Pereira, F. D., Parfenov, V. A., Sun, Y., Wang, Q., Akhmedova, S. A., Sviridova, I. K. et al. (2017). Bioprinting of a functional vascularized mouse thyroid gland construct. *Biofabrication* **9**, 034105. doi:10.1088/1758-5090/aa7fdd

Burris, R. E. and Hebrok, M. (2007). Pancreatic innervation in mouse development and β-cell regeneration. *Neuroscience* **150**, 592-602. doi:10.1016/j.neuroscience.2007.09.079

Chen, M. J., Yokomizo, T., Zeigler, B. M., Dzierzak, E. and Speck, N. A. (2009). Runx1 is required for the endothelial to haematopoietic cell transition but not thereafter. *Nature* **457**, 887-891. doi:10.1038/nature07619

Chung, K., Wallace, J., Kim, S.-Y., Kalyanasundaram, S., Andalman, A. S., Davidson, T. J., Mirzabekov, J. J., Zalocusky, K. A., Mattis, J., Denisin, A. K. et al. (2013). Structural and molecular interrogation of intact biological systems. *Nature* **497**, 332-337. doi:10.1038/nature12107

Cozzitorto, C. and Spagnoli, F. M. (2019). Pancreas organogenesis: the interplay between surrounding microenvironment(s) and epithelium-intrinsic factors. *Curr. Top. Dev. Biol.* **132**, 221-256. doi:10.1016/bs.ctdb.2018.12.005

Cozzitorto, C., Mueller, L., Ruzittu, S., Mah, N., Willnow, D., Darrigrand, J.-F., Wilson, H., Khosravinia, D., Mahmoud, A.-A., Risolino, M. et al. (2020). A specialized Niche in the pancreatic microenvironment promotes endocrine differentiation. *Dev. Cell* **55**, 150-162.e56. doi:10.1016/j.devcel.2020.08.003

de Medeiros, G., Balázs, B. and Hufnagel, L. (2016). Light-sheet imaging of mammalian development. *Semin. Cell Dev. Biol.* **55**, 148-155. doi:10.1016/j.semcdb.2015.11.001

Esni, F., Johansson, B. R., Radice, G. L. and Semb, H. (2001). Dorsal pancreas agenesis in N-cadherin- deficient mice. *Dev. Biol.* **238**, 202-212. doi:10.1006/dbio.2001.0405

Fowler, J. L., Lee, S. S.-Y., Wesner, Z. C., Olehnik, S. K., Kron, S. J. and Hara, M. (2018). Three-dimensional analysis of the human pancreas. *Endocrinology* **159**, 1393-1400. doi:10.1210/en.2017-03076

Gittes, G. K. (2009). Developmental biology of the pancreas: a comprehensive review. *Dev. Biol.* **326**, 4-35. doi:10.1016/j.ydbio.2008.10.024

Golosow, N. and Grobstein, C. (1962). Epitheliomesenchymal interaction in pancreatic morphogenesis. *Dev. Biol.* **4**, 242-255. doi:10.1016/0012-1606(62)90042-8

Gonay, L., Spourquet, C., Baudoin, M., Lepers, L., Lemoine, P., Fletcher, A. G., Hanert, E. and Pierreux, C. E. (2021). Modelling of epithelial growth, fission and lumen formation during embryonic thyroid development: a combination of computational and experimental approaches. *Front. Endocrinol.* **12**, 655862. doi:10.3389/fendo.2021.655862

Harari, N., Sakhneny, L., Khalifa-Malka, L., Busch, A., Hertel, K. J., Hebrok, M. and Landsman, L. (2019). Pancreatic pericytes originate from the embryonic pancreatic mesenchyme. *Dev. Biol.* **449**, 14-20. doi:10.1016/j.ydbio.2019.01.020

Herrera, P.-L., Orci, L. and Vassalli, J.-D. (1998). Two transgenic approaches to define the cell lineages in endocrine pancreas development. *Mol. Cell. Endocrinol.* **140**, 45-50. doi:10.1016/S0303-7207(98)00028-8

Heymans, C., Degosserie, J., Spourquet, C. and Pierreux, C. E. (2019). Pancreatic acinar differentiation is guided by differential laminin deposition. *Sci. Rep.* **9**, 2711. doi:10.1038/s41598-019-39077-6

Hick, A.-C., van Eyll, J. M., Cordi, S., Forez, C., Passante, L., Kohara, H., Nagasawa, T., Vanderhaeghen, P., Courtoy, P. J., Rousseau, G. G. et al. (2009). Mechanism of primitive duct formation in the pancreas and submandibular glands: a role for SDF-1. *BMC Dev. Biol.* **9**, 66. doi:10.1186/1471-213X-9-66

Hingorani, S. R., Petricoin, E. F., Maitra, A., Rajapakse, V., King, C., Jacobetz, M. A., Ross, S., Conrads, T. P., Veenstra, T. D., Hitt, B. A. et al. (2003). Preinvasive and invasive ductal pancreatic cancer and its early detection in the mouse. *Cancer Cell* **4**, 437-450. doi:10.1016/S1535-6108(03)00309-X

Iber, D., Karimaddini, Z. and Ünal, E. (2016). Image-based modelling of organogenesis. *Brief. Bioinform.* **17**, 616-627. doi:10.1093/bib/bbv093

Jacquemin, P., Yoshitomi, H., Kashima, Y., Rousseau, G. G., Lemaigre, F. P. and Zaret, K. S. (2006). An endothelial-mesenchymal relay pathway regulates early phases of pancreas development. *Dev. Biol.* **290**, 189-199. doi:10.1016/j.ydbio.2005.11.023

Jørgensen, M. C., Ahnfelt-Rønne, J., Hald, J., Madsen, O. D., Serup, P. and Hecksher-Sørensen, J (2007). An illustrated review of early pancreas development in the mouse. *Endocr. Rev.* **28**, 685-705. doi:10.1210/er.2007-0016

Kaufman-Francis, K., Koffler, J., Weinberg, N., Dor, Y. and Levenberg, S. (2012). Engineered vascular beds provide key signals to pancreatic hormone-producing cells. *PLoS ONE* **7**, e40741. doi:10.1371/journal.pone.0040741

Kesavan, G., Sand, F. W., Greiner, T. U., Johansson, J. K., Kobberup, S., Wu, X., Brakebusch, C. and Semb, H. (2009). Cdc42-mediated tubulogenesis controls cell specification. *Cell* **139**, 791-801. doi:10.1016/j.cell.2009.08.049

Kesavan, G., Lieven, O., Mamidi, A., Öhlin, Z. L., Johansson, J. K., Li, W.-C., Lommel, S., Greiner, T. U. and Semb, H. (2014). Cdc42/N-WASP signaling links actin dynamics to pancreatic β cell delamination and differentiation. *Development* **141**, 685-696. doi:10.1242/dev.100297

Khairy, K. and Keller, P. J. (2011). Reconstructing embryonic development. *Genesis* **49**, 488-513. doi:10.1002/dvg.20698

Kretzschmar, K. and Watt, F. M. (2012). Lineage tracing. *Cell* **148**, 33-45. doi:10.1016/j.cell.2012.01.002

Lammert, E., Cleaver, O. and Melton, D. (2001). Induction of pancreatic differentiation by signals from blood vessels. *Science* **294**, 564-567. doi:10.1126/science.1064344

Lammert, E., Gu, G., McLaughlin, M., Brown, D., Brekken, R., Murtaugh, L. C., Gerber, H.-P., Ferrara, N. and Melton, D. A. (2003). Role of VEGF-A in vascularization of pancreatic islets. *Curr. Biol.* **13**, 1070-1074. doi:10.1016/S0960-9822(03)00378-6

Landsman, L., Nijagal, A., Whitchurch, T. J., Vanderlaan, R. L., Zimmer, W. E., Mackenzie, T. C. and Hebrok, M. (2011). Pancreatic mesenchyme regulates

DEVELOPMENT

epithelial organogenesis throughout development. *PLoS Biol.* **9**, e1001143. doi:10.1371/journal.pbio.1001143

Larsen, H. L. and Grapin-Botton, A. (2017). The molecular and morphogenetic basis of pancreas organogenesis. *Semin. Cell Dev. Biol.* **66**, 51-68. doi:10.1016/j.semcdb.2017.01.005

Larsen, H. L., Martín-Coll, L., Nielsen, A. V., Wright, C. V. E., Trusina, A., Kim, Y. H. and Grapin-Botton, A. (2017). Stochastic priming and spatial cues orchestrate heterogeneous clonal contribution to mouse pancreas organogenesis. *Nat. Commun.* **8**, 605. doi:10.1038/s41467-017-00258-4

Magenheim, J., Ilovich, O., Lazarus, A., Klochendler, A., Ziv, O., Werman, R., Hija, A., Cleaver, O., Mishani, E., Keshet, E. et al. (2011). Blood vessels restrain pancreas branching, differentiation and growth. *Development* **138**, 4743-4752. doi:10.1242/dev.066548

Mamidi, A., Prawiro, C., Seymour, P. A., de Lichtenberg, K. H., Jackson, A., Serup, P. and Semb, H. (2018). Mechanosignalling via integrins directs fate decisions of pancreatic progenitors. *Nature* **564**, 114-118. doi:10.1038/s41586-018-0762-2

Muzumdar, M. D., Tasic, B., Miyamichi, K., Li, L. and Luo, L. (2007). A global double-fluorescent Cre reporter mouse. *Genesis* **45**, 593-605. doi:10.1002/dvg.20335

Nikolova, G., Jabs, N., Konstantinova, I., Domogatskaya, A., Tryggvason, K., Sorokin, L., Fässler, R., Gu, G., Gerber, H.-P., Ferrara, N. et al. (2006). The vascular basement membrane: a niche for insulin gene expression and β cell proliferation. *Dev. Cell* **10**, 397-405. doi:10.1016/j.devcel.2006.01.015

Pan, F. C. and Wright, C. (2011). Pancreas organogenesis: from bud to plexus to gland. *Dev. Dyn.* **240**, 530-565. doi:10.1002/dvdy.22584

Petzold, K. M., Naumann, H. and Spagnoli, F. M. (2013). Rho signalling restriction by the RhoGAP Stard13 integrates growth and morphogenesis in the pancreas. *Development (Cambridge, England)* **140**, 126-135. doi:10.1242/dev.082701

Pierreux, C. E., Cordi, S., Hick, A.-C., Achouri, Y., Ruiz de Almodovar, C., Prévot, P.-P., Courtoy, P. J., Carmeliet, P. and Lemaigre, F. P. (2010). Epithelial: endothelial cross-talk regulates exocrine differentiation in developing pancreas. *Dev. Biol.* **347**, 216-227. doi:10.1016/j.ydbio.2010.08.024

Puri, S. and Hebrok, M. (2007). Dynamics of embryonic pancreas development using real-time imaging. *Dev. Biol.* **306**, 82-93. doi:10.1016/j.ydbio.2007.03.003

Richardson, D. S. and Lichtman, J. W. (2015). Clarifying tissue clearing. *Cell* **162**, 246-257. doi:10.1016/j.cell.2015.06.067

Roostalu, U., Lercke Skytte, J., Gravesen Salinas, C., Klein, T., Vrang, N., Jelsing, J. and Hecksher-Sørensen, J. (2020). 3D quantification of changes in pancreatic islets in mouse models of diabetes type I and II. *Dis. Model. Mech.* **13**, dmm045351. doi:10.1242/dmm.045351

Sakhneny, L., Khalifa-Malka, L. and Landsman, L. (2019). Pancreas organogenesis: Approaches to elucidate the role of epithelial-mesenchymal interactions. *Semin. Cell Dev. Biol.* **92**, 89-96. doi:10.1016/j.semcdb.2018.08.012

Sand, F. W., Hörnblad, A., Johansson, J. K., Lorén, C., Edsbagge, J., Ståhlberg, A., Magenheim, J., Ilovich, O., Mishani, E., Dor, Y. et al. (2011). Growth-limiting role of endothelial cells in endoderm development. *Dev. Biol.* **352**, 267-277. doi:10.1016/j.ydbio.2011.01.026

Saunders, D. C., Messmer, J., Kusmartseva, I., Beery, M. L., Yang, M., Atkinson, M. A., Powers, A. C., Cartailler, J.-P. and Brissova, M. (2020). Pancreatlas: applying an adaptable framework to map the human pancreas in health and disease. *Patterns* **1**, 100120. doi:10.1016/j.patter.2020.100120

Seymour, P. A. and Serup, P. (2019). Mesodermal induction of pancreatic fate commitment. *Semin. Cell Dev. Biol.* **92**, 77-88. doi:10.1016/j.semcdb.2018.08.008

Shah, S. R., Esni, F., Jakub, A., Paredes, J., Lath, N., Malek, M., Potoka, D. A., Prasadan, K., Mastroberardino, P. G., Shiota, C. et al. (2011). Embryonic

mouse blood flow and oxygen correlate with early pancreatic differentiation. *Dev. Biol.* **349**, 342-349. doi:10.1016/j.ydbio.2010.10.033

Sharon, N., Chawla, R., Mueller, J., Vanderhooft, J., Whitehorn, L. J., Rosenthal, B., Gürtler, M., Estanboulieh, R. R., Shvartsman, D., Gifford, D. K. et al. (2019). A peninsular structure coordinates asynchronous differentiation with morphogenesis to generate pancreatic islets. *Cell* **176**, 790-804.e13. doi:10.1016/j.cell.2018.12.003

Shih, H. P., Wang, A. and Sander, M. (2013). Pancreas organogenesis: from lineage determination to morphogenesis. *Annu. Rev. Cell Dev. Biol.* **29**, 81-105. doi:10.1146/annurev-cellbio-101512-122405

Sneddon, J. B., Tang, Q., Stock, P., Bluestone, J. A., Roy, S., Desai, T. and Hebrok, M. (2018). Stem cell therapies for treating diabetes: progress and remaining challenges. *Cell Stem Cell* **22**, 810-823. doi:10.1016/j.stem.2018.05.016

Snyder, C. S., Harrington, A. R., Kaushal, S., Mose, E., Lowy, A. M., Hoffman, R. M. and Bouvet, M. (2013). A dual-color genetically engineered mouse model for multispectral imaging of the pancreatic microenvironment. *Pancreas* **42**, 952-958. doi:10.1097/MPA.0b013e31828643df

Stanley, E. G., Biben, C., Elefanty, A., Barnett, L., Koentgen, F., Robb, L. and Harvey, R. P. (2002). Efficient Cre-mediated deletion in cardiac progenitor cells conferred by a 3'UTR-ires-Cre allele of the homeobox gene Nkx2-5. *Int. J. Dev. Biol.* **46**, 431-439.

Susaki, E. A., Tainaka, K., Perrin, D., Kishino, F., Tawara, T., Watanabe, T. M., Yokoyama, C., Onoe, H., Eguchi, M., Yamaguchi, S. et al. (2014). Whole-brain imaging with single-cell resolution using chemical cocktails and computational analysis. *Cell* **157**, 726-739. doi:10.1016/j.cell.2014.03.042

Swoger, J., Pampaloni, F. and Stelzer, E. H. K. (2014). Light-sheet-based fluorescence microscopy for three-dimensional imaging of biological samples. *Cold Spring Harb. Protoc.* **2014**, 1-8. doi:10.1101/pdb.top080168

Sznurkowska, M. K., Hannezo, E., Azzarelli, R., Rulands, S., Nestorowa, S., Hindley, C. J., Nichols, J., Göttgens, B., Huch, M., Philpott, A. et al. (2018). Defining lineage potential and fate behavior of precursors during pancreas development. *Dev. Cell* **46**, 360-375.e65. doi:10.1016/j.devcel.2018.06.028

Verzi, M. P., Stanfel, M. N., Moses, K. A., Kim, B.-M., Zhang, Y., Schwartz, R. J., Shivdasani, R. A. and Zimmer, W. E. (2009). Role of the homeodomain transcription factor Bapx1 in mouse distal stomach development. *Gastroenterology* **136**, 1701-1710. doi:10.1053/j.gastro.2009.01.009

Villasenor, A., Chong, D. C., Henkemeyer, M. and Cleaver, O. (2010). Epithelial dynamics of pancreatic branching morphogenesis. *Development (Cambridge, England)* **137**, 4295-4305. doi:10.1242/dev.052993

Wan, Y., McDole, K. and Keller, P. J. (2019). Light-sheet microscopy and its potential for understanding developmental processes. *Annu. Rev. Cell Dev. Biol.* **35**, 655-681. doi:10.1146/annurev-cellbio-100818-125311

Wessells, N. K. and Cohen, J. H. (1967). Early pancreas organogenesis: morphogenesis, tissue interactions, and mass effects. *Dev. Biol.* **15**, 237-270. doi:10.1016/0012-1606(67)90042-5

Yung, T., Poon, F., Liang, M., Coquenlorge, S., McGaugh, E. C., Hui, C.-C., Wilson, M. D., Nostro, M. C. and Kim, T.-H. (2019). Sufu- and Spop-mediated downregulation of Hedgehog signaling promotes beta cell differentiation through organ-specific niche signals. *Nat. Commun.* **10**, 4647. doi:10.1038/s41467-019-12624-5

Zhou, Q., Law, A. C., Rajagopal, J., Anderson, W. J., Gray, P. A. and Melton, D. A. (2007). A multipotent progenitor domain guides pancreatic organogenesis. *Dev. Cell* **13**, 103-114. doi:10.1016/j.devcel.2007.06.001

Zorn, A. M. and Wells, J. M. (2009). Vertebrate endoderm development and organ formation. *Annu. Rev. Cell Dev. Biol.* **25**, 221-251. doi:10.1146/annurev.cellbio.042308.113344
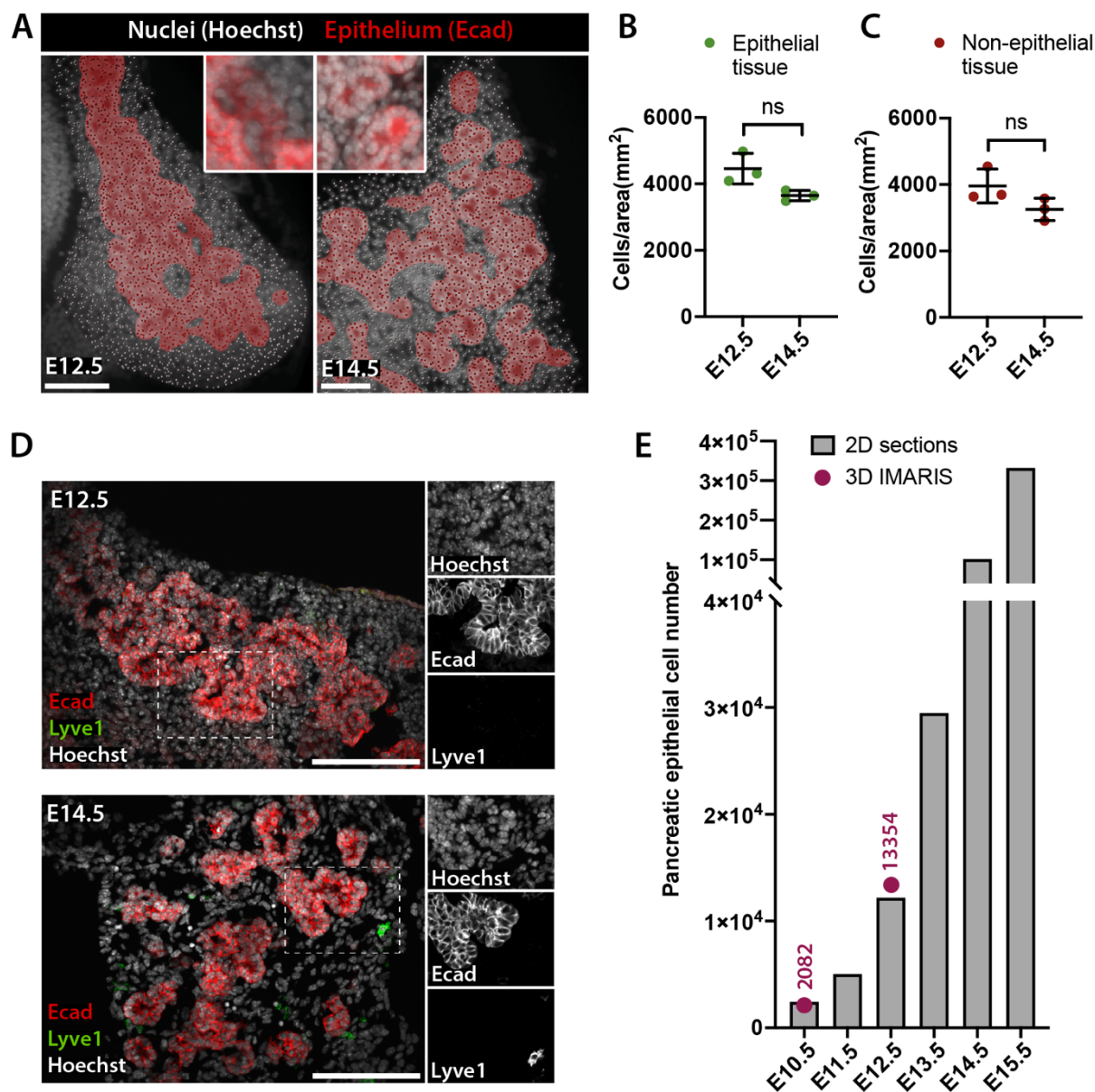
DEVELOPMENT

Fig. S1. Analysis of LSFM scans of embryonic pancreas.

(A) Cell density in pancreatic epithelium (Ecad$^+$) and non-epithelial tissues was measured on optical sections from LSFM scans of E12.5 and E14.5 embryonic pancreata using the Imaris software. Tissues were stained with antibodies against Ecad to distinguish the pancreatic epithelium and Hoechst as nuclear counterstain. Scale bar, 50 μm. **(B, C)** Scatter plot showing quantification of cells per area in epithelial (B) and non-epithelial tissues (C) at E12.5 (n=3) and E14.5 (n=3). Epithelial and non-epithelial areas were measured using the manual 'Surface creation' module and nuclei were detected using the 'Spots creation' module. For each embryo,

optical sections were analysed at regular intervals (E12.5, every 30µm: E14.5, every 60µm) throughout the entire pancreatic tissue to calculate the average cell density. Overall cell density in epithelial and non-epithelial pancreatic tissues was unchanged between E12.5 and E14.5 pancreata. **(D)** Representative IF images of pancreatic tissue sections at E12.5 (A) and E14.5 (B). IF labelling for the Lymphatic vessel endothelial hyaluronan receptor 1 (Lyve1; green) marks rare lymphatic cells in the embryonic pancreas. Ecad (red) demarcates the pancreatic epithelium. Hoechst (grey) was used as nuclear counterstain. Insets show higher magnifications of the boxed regions as single channel configuration. Scale bars, 100 µm. **(E)** Measurement of epithelial cell number in the dorsal pancreas from E10.5 to E15.5 using Halo software and Imaris software. Total epithelial cell number was determined with HALO software by integrating the number of epithelial cells (Ecad$^+$) computed on regularly spaced 2D sections (every 30 µm) spanning the whole pancreatic anlages (Gonay et al., 2021). 3D Imaris quantification (red) was performed using 'Spots' segmentation on epithelial cells (Ecad$^+$ or Pdx1$^+$) of the entire pancreatic tissue at stage E10.5 and E12.5.
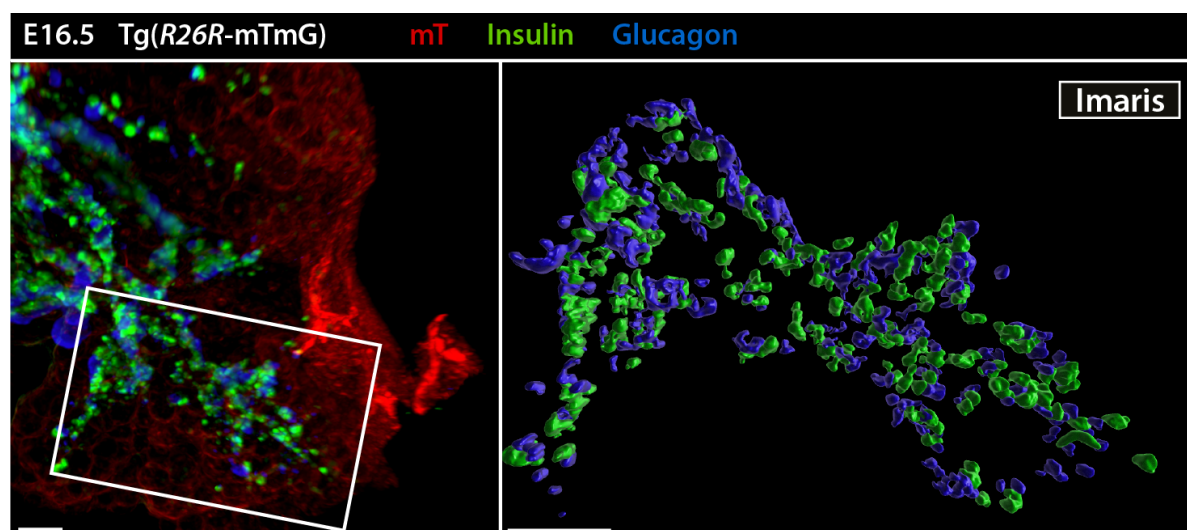
Fig. S2. LSFM images of pancreas endocrine tissue. Representative LSFM 3D image (left) and Imaris surface rendering (right) of the pancreas from Tg(*R26R*-mTmG) embryos at E16.5. WMIF for insulin (green) and glucagon (blue) labels the pancreatic beta- and alpha- endocrine cells, respectively. mT (red) mark all cell membranes. Right panel, surface rendered 3D model of the boxed area showing insulin[+] and glucagon^{+} cells adjacent to each other, arranged in a peninsular structure with peripheral glucagon^{+} cells and internal insulin^{+} cells. Scale bars, 100 μm.
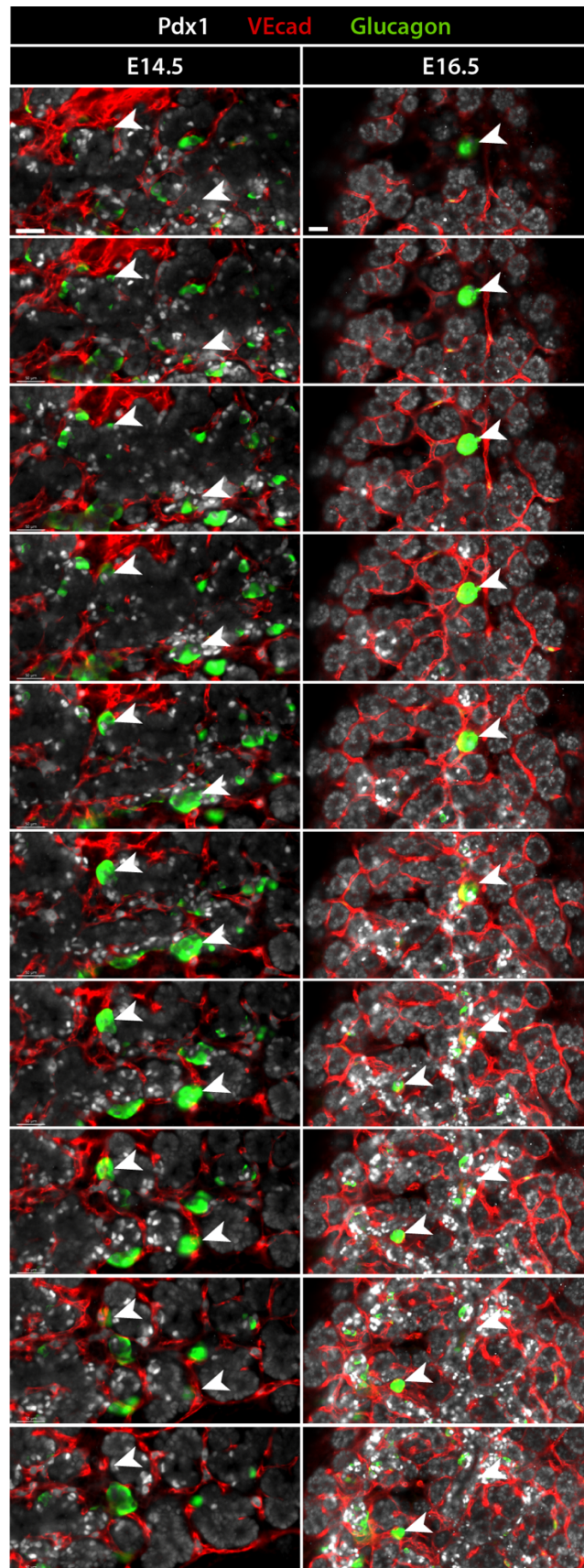
Fig. S3. LSFM scans of pancreas endocrine tissue. Representative consecutive optical sections (separated by 10 μm) through E14.5 and E16.5 pancreas after LSFM imaging, showing Pdx1+ pancreatic cells (grey), VEcad+ endothelial cells (red) and glucagon+ cells (green). Arrowheads indicate glucagon+ clusters arising from the epithelium surrounded by vessels. Scale bar, 50 μm.

Fig. S4. Schematic representation of data collection and deposition. Flowchart describing the experimental steps used to generate the image dataset presented here and the organizational structure of the online data repository in which they can be accessed.

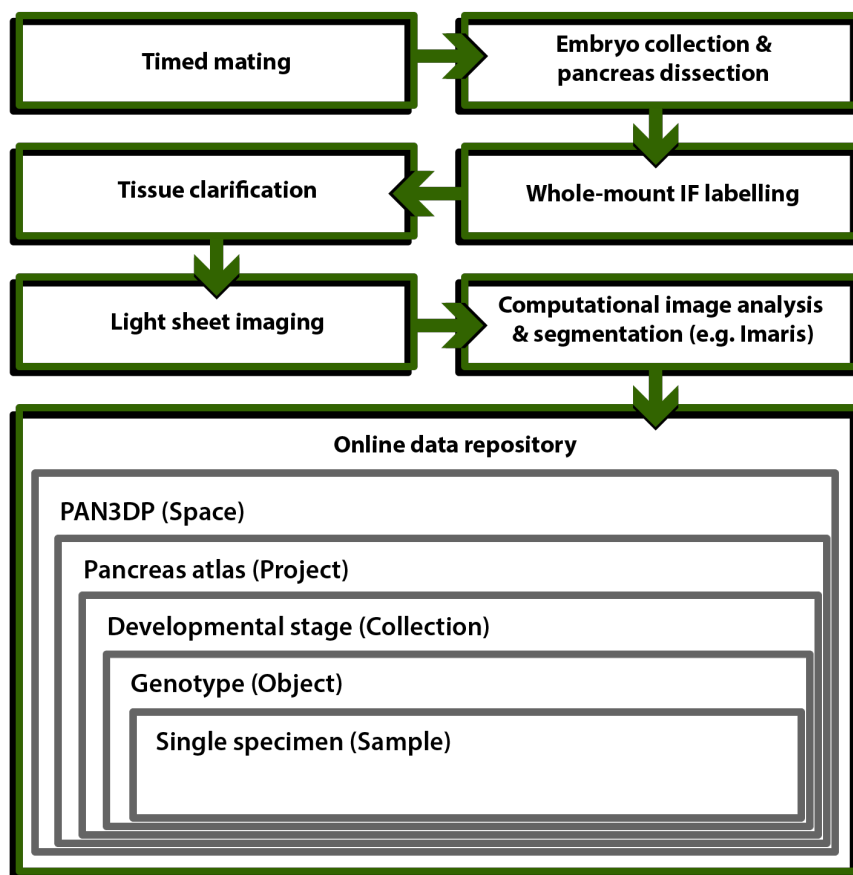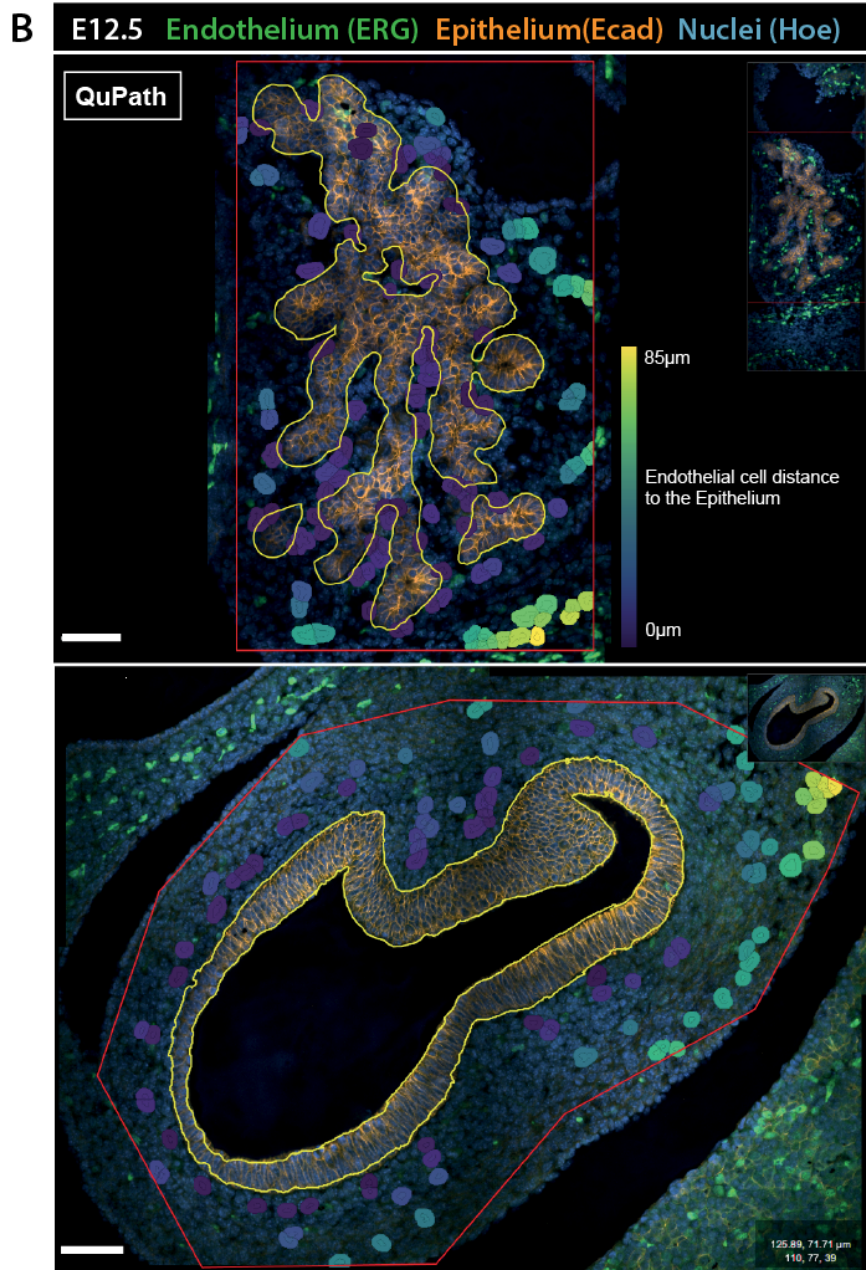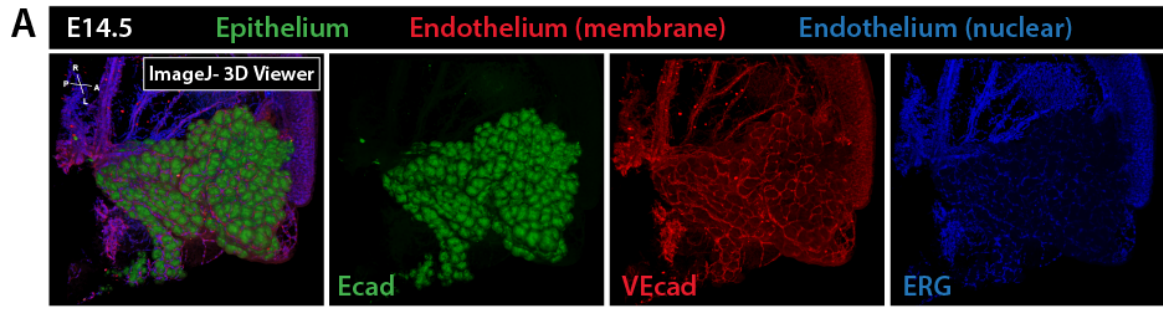**Fig. S5. Visualisation and analysis of LSFM 3D images of pancreatic tissue using open- source software. (A)** Representative LSFM 3D images of the E14.5 wildtype pancreas shown in Fig. 3B visualized using the 3D Viewer plugin in ImageJ. WMIF for Ecad (green), VEcad (red) and ERG (blue). 3D images and surface renderings are shown as merged (leftmost panel) and individual channels (right panels). A, anterior; P, posterior; L, left; R, right. **(B)** Quantitative analysis of endothelial cell distribution around the pancreatic epithelium using QuPath. QuPath rendering of the E12.5 pancreas and stomach sections shown in Fig. 4G. E- cadherin (Ecad) labelling is shown in orange, ERG in green and Hoechst in blue. ERG positive endothelial cells are pseudocolored using the "Distance to annotation" tool. Endothelial cells pseudocolour follow the Viridis palette according to their distance from the epithelium ($Ecad^+$ region).

Table S1. Data deposited in the Pancreas Embryonic Cell Atlas.

Stage	All nuclei		Epithelial cells			Endothelial cells				Mesenchymal cells		Endocrine Cells				No of images
	DRAQ5	HOECHST	Pdx1	Pdx1-Cre mTmG	E-Cadherin	VE-Cadherin	ERG	Sox17	Cdh5-Cre mTmG	Nkx2.5-Cre mTmG	Nkx2.5-Cre H2B	Glucagon	Ins2-Cre mTmG	Insulin	Pax6	
E12.5					green	orange										3
E12.5		blue	orange		green	green										7
E12.5			orange			green										1
E12.5			purple	green												4
E12.5			green					orange								1
E12.5			purple		purple											3
E12.5			purple							green						6
E12.5		blue			green	orange	purple									2
E12.5		blue	orange													1
E12.5		blue			purple								green			4
E12.5		blue							green							3
E14.5		blue			green	orange	purple									4
E14.5	purple	blue	orange													4
E14.5			purple							green						5
E14.5					green	orange	purple									3
E14.5		blue	green			orange						purple				2
E14.5		blue	purple			orange									green	1
E14.5						orange					green	purple				3
E16.5		blue	purple			orange						green				2
E16.5		blue				orange					green	purple				2
E16.5		blue				orange						purple		green		1
E16.5		blue	purple			orange									green	1
E16.5		blue										purple	green			1
E18.5		blue	green			orange						purple				1
P0		blue	purple			orange						green				1

Colour	Wavelength
blue	405 nm
green	488 nm
orange	568 nm
purple	647 nm

Table S2. Antibodies and fluorescent dyes

Name	Company	Catalog Number	Dilution
Rat anti-E-CADHERIN	Sigma	U3254	1:500
Rabbit anti-ERG	Abcam	Ab92513	1:100
Chicken anti-GFP	Aves	GFP-1020	1:400
Rabbit anti-Glucagon	Immunostar Inc.	20076	1:500
Guinea pig anti-Insulin	Agilent/Dako	A0564	1:300
Guinea pig anti-PDX1	Abcam	Ab47308	1:500
Rat anti-RFP	Antikörper online	ABIN334653	1:400
Goat anti-SOX17	R&D Systems	AF1924	1:200
Goat anti-VE-CADHERIN	R&D Systems	AF1002-SP	1:50
Donkey Alexa Fluor 488-labelled Anti-Goat IgG	Invitrogen	A11055	1:1000
Donkey Alexa Fluor 488-labelled Anti-Guinea Pig IgG	Dianova	706-545-148	1:1000
Donkey Alexa Fluor 488-labelled Anti-Rat IgG	Invitrogen	A21208	1:1000
Goat Alexa Fluor 488-labelled Anti-Chicken IgG	Invitrogen	A11039	1:1000
Donkey Alexa Fluor 568-labelled Anti-Goat IgG	Invitrogen	A11057	1:1000
Donkey Alexa Fluor 594-labelled Anti-Rat IgG	Invitrogen	A21209	1:1000
Goat Alexa Fluor 568-labelled Anti-Guinea Pig IgG	Invitrogen	A11075	1:1000
Donkey Alexa Fluor 647-labelled Anti-Guinea Pig IgG	Dianova	706-605-148	1:1000
Donkey Alexa Fluor 647-labelled Anti-Rabbit IgG	Invitrogen	A31573	1:1000
Donkey Alexa Fluor 647-labelled Anti-Rat IgG	Dianova	712-605-153	1:1000
eBioscience™ DRAQ5™	Invitrogen	65-0880-96	1:500
Hoechst 33342	Invitrogen	H1399	1:1000